The Marinoan cap carbonate of Svalbard: Syngenetic marine dolomite with ^{17}O-anomalous carbonateassociated sulphate

Journal Item

Received: 24 April 2022 | Revised: 14 June 2022 | Accepted: 14 June 2022

DOI: 10.1002/dep2.201

The Depositional Record Open Access
A journal of the International Association of Sedimentologists
WILEY

ORIGINAL ARTICLE

The Marinoan cap carbonate of Svalbard: Syngenetic marine dolomite with ^{17}O-anomalous carbonate-associated sulphate

Ian J. Fairchild[1] | **Huiming Bao**[2,3] | **Richard J. Windmill**[1,4] | **Ian Boomer**[1]

[1]School of Geography, Earth and Environmental Sciences, University of Birmingham, Birmingham, UK

[2]International Center for Isotope Effects Research (ICIER), Nanjing University, Nanjing, China

[3]School of Earth Sciences and Engineering, Nanjing University, Nanjing, China

[4]Planetary and Space Sciences, School of Physical Sciences, The Open University, Milton Keynes, UK

Correspondence
Ian J. Fairchild, School of Geography, Earth and Environmental Sciences, University of Birmingham, Birmingham B15 2TT, UK.
Email: i.j.fairchild@bham.ac.uk

Funding information
Natural Environment Research Council, Grant/Award Number: NE/H004963/1

Abstract

Two cap carbonates overlying Cryogenian panglacial deposits are found in North-East Svalbard of which the younger (635 Ma) forms the base of the Ediacaran Period. It is represented by a transgressive succession in which laminated dolostone, typically around 20 m thick (Member D1), is succeeded transitionally by a similar thickness of impure carbonates (Member D2). In Spitsbergen, there is evidence of microbially influenced sediment stabilisation and carbonate precipitation in the lower part of D1, whilst the upper part of D1 and D2 show centimetre-decimetre-scale graded units with undulatory lamination interpreted as evidence of storm activity. Carbonate originated as possible freshwater whitings, as well as microbial precipitates. Exhumed and eroded hardgrounds display replacive 10–30 μm dolomite crystals with cathodoluminescence characteristics consistent with early diagenetic manganese and iron reduction. Regionally, carbon isotope values consistently decrease by around 2‰ from around −3‰ over 30 m of section which is both a temporal and a bathymetric signal, but not a global one. An exponential decline in carbonate production predicted by box models is fitted by a semi-quantitative sedimentation model. A mass-anomalous ^{17}O depletion in carbonate-associated sulphate in dolomite, inherited from precursor calcite, decreases from −0.6 to −0.3‰ in the basal 15 m of section and then approaches background values. The post-glacial anomalous ^{17}O depletion in carbonate-associated sulphate and barite elsewhere has been interpreted in terms of ultra-high pCO_2 at the onset of deglaciation. Such anomalies, with larger amplitude, have been reported in Svalbard from underlying lacustrine and tufaceous limestones representing a hyperarid glacial environment. The anomalous sulphate could be produced contemporarily, or the internally drained landscape may have continued to release ^{17}O-anomalous sulphate as it was transgressed during cap carbonate deposition. The late Cryogenian to earliest Ediacaran record in Svalbard provides the most complete record of the basal ^{17}O-depletion event in the world.

KEYWORDS
^{17}O, cap carbonate, carbonate-associated sulphate, dolomite, Ediacaran, Svalbard

1 | INTRODUCTION

Proterozoic carbonates are predominantly dolomitic, reflecting the capacity for contemporary seawater to form dolomite (Hood & Wallace, 2018; Tucker, 1982). The rapid stabilisation of mineralogy and an absence of disturbance by metazoans makes these rocks excellent archives of sedimentary environments and marine geochemistry. A special feature in the Cryogenian Period (720–635 Ma) is the association of carbonates with glacigenic deposits (Fairchild, 1993), which is primarily due to glaciers extending to low palaeolatitudes in two episodes of panglaciation (Hoffman et al., 2017). The consequences include the incorporation of carbonate debris from the erosion of underlying sediments and the local precipitation of carbonates in glaciolacustrine and glaciomarine settings (Spence et al., 2016). In addition, the glacial units are normally overlain by a 1–50 m cap carbonate, even in otherwise non-carbonate successions.

In Snowball Earth theory, as articulated by Hoffman et al. (1998) and Hoffman and Schrag (2002), and underpinned by climate modelling (Budyko, 1969; Voigt & Abbot, 2012), cap carbonates form at the end of a prolonged glaciation in which ice coverage of the planet inhibited consumption of atmospheric carbon dioxide by weathering. They represent the result of titration of high atmospheric CO_2 in a hothouse climate accompanying deglaciation and eustatic sea-level rise over a few thousand years. Several aspects of the theory have been vindicated by subsequent work:

a. Cryogenian glaciations were severe, true panglaciations (Marinoan sea level lowered by *ca* 600 m) and both are present on all main continental blocks (Hoffman et al., 2017, 2021).
b. The two Cryogenian panglaciations were long-lasting (Sturtian 55 Myr and Marinoan at least 5 Myr, Prave et al., 2016; Zhou et al., 2019).
c. PCO_2 was high by the close of the Marinoan glaciation (Bao et al., 2008, 2009).

However, in the terrestrial realm, glacial advances and retreats have been documented late in the Marinoan ice age when PCO_2 was high and these were linked to model solutions of Milankovitch forcing (Benn et al., 2015). In the marine realm, the persistence of ice cover throughout the glaciation is directly contradicted by sedimentological evidence of open water within glacigenic deposits of both Sturtian (Spence et al., 2016) and Marinoan (Lang et al., 2018) times.

The meaning of cap carbonates is contested (Fairchild & Kennedy, 2007; Yu et al., 2020), although there is agreement that they accumulated during major marine transgression. In this immediately post-glacial period, Shields (2005) predicted a 'plumeworld' with a kilometre-scale freshwater lid on the ocean as a consequence of the insistence of climate models of Snowball Earth that the final meltdown would be very rapid. The carbonate facies are distinctive, implying some unique characteristics, but the link with atmospheric CO_2 drawdown has been challenged (Huang et al., 2016) and alternative models, such as deposition on sediment-starved platforms over $>10^5$ years have been developed (Kennedy & Christie-Blick, 2011; Nordsvan et al., 2019). The post-glacial carbon isotope anomaly shows more complex features than originally thought and is the subject of many competing hypotheses. Recently, there has been an intense focus on trying out new geochemical proxies on the post-glacial successions, but not all these works consider how the geochemical signals might be influenced by sedimentological setting and diagenesis. Complementary biogeochemical and/or diagenetic modelling provide useful insights (Ahm et al., 2019), but the bundling of the underlying assumptions in the model structure can be difficult to unpick. A basic issue is how do cap carbonates, with apparently marine chemistry (Halverson et al., 2004), relate to the proposed thick post-glacial freshwater lens (Shields, 2005; Yang et al., 2017)?

In this paper, new evidence is presented about the nature of a cap carbonate from Svalbard, which is then interpreted in relation to a wealth of recent literature on such deposits. Previous sedimentological and geochemical descriptions (Fairchild & Hambrey, 1984; Halverson et al., 2004) remain valid, but are supplemented by data from more recent fieldwork and sample re-analysis, allowing novel interpretations. The key new observations are (i) field and petrographic observations providing evidence for dolomite formation in syn-depositional marine diagenesis (cf. Wallace et al., 2019) and (ii) demonstration of a stratigraphic negative $\Delta^{17}O_{SO4}$ anomaly in carbonate-associated sulphate (CAS). This is only the second example of such an anomaly found in a cap carbonate (cf. Bao et al., 2012). Furthermore, Svalbard is the only location where the anomaly is present in the underlying Marinoan deposits where it has been used to infer high syn-glacial carbon dioxide levels when the sulphate was created (Bao et al., 2009; Benn et al., 2015). Additionally, insights into sediment accumulation rates allows a reconciliation

between the traditionally contrasting models of rapid versus slow cap carbonate formation.

2 | REGIONAL GEOLOGY AND PREVIOUS WORK

Geographically the study area is in the regions of Olav V Land and Ny Friesland in the north-east of Spitsbergen, the main island of the Svalbard group. Published data by others from coastal areas of the nearby island of Nordaustlandet (Figure 1) are also referred to. Stratigraphically, the Polarisbreen Group (Figure 2) encompasses the Cryogenian Period and ranges from late Tonian to mid-Ediacaran.

The Polarisbreen Group conformably overlies a thick (>6 km) pile of Neoproterozoic shallow marine deposits, resting on older metasediments, and represents the post-rifting thermal subsidence phase of an intracratonic basin on the margin of Rodinia. Stratigraphic continuity of many marker horizons across to North-East Greenland and the paucity of local changes in stratigraphic thickness may indicate deposition along the strike of the basin margin (Fairchild & Hambrey, 1995; Halverson, 2011; Halverson et al., 2018; Knoll et al., 1986).

New Re–Os dates (Millikin et al., 2022) demonstrate the correlation of the two sharply defined Neoproterozoic glacigenic units in the Polarisbreen Group (Fairchild & Hambrey, 1984; Halverson, 2011) with the two Cryogenian panglaciations. These first-order disturbances in Earth history are widely known as the Sturtian (717–660 Ma) and Marinoan (?651/640 to 635 Ma) episodes (Halverson et al., 2020; Zhou et al., 2019). The correlation of local with global events

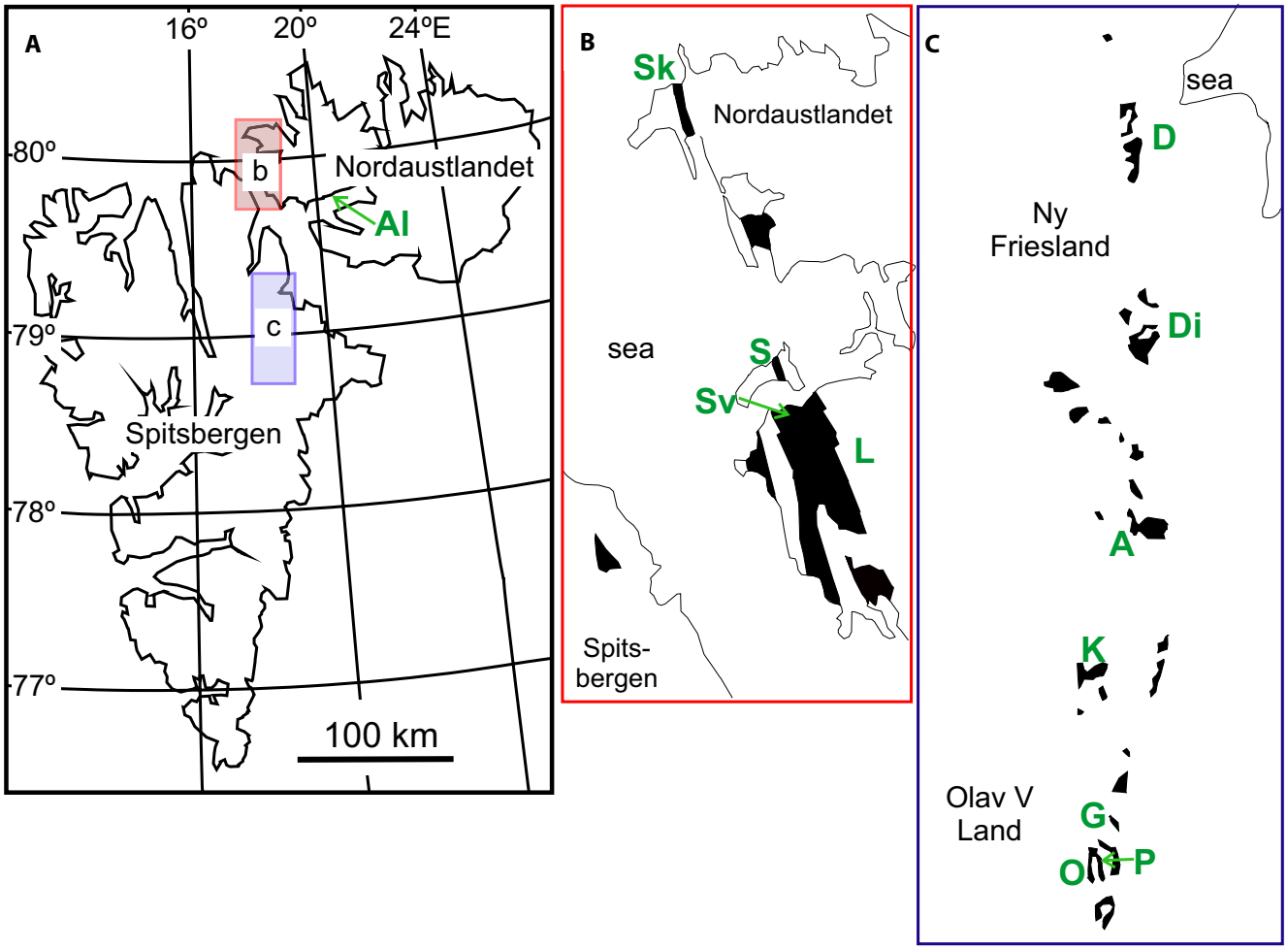

FIGURE 1 (A) Map of Svalbard showing location of Aldousbreen (Al, Edwards, 1976) and boxes b. and c. (B) Nordaustlandet locations described by Halverson et al. (2004). L, Liljequisthøgda; Sv, Sveanor (Backaberget on Norsk Polarinstitutt maps); S, Søre Russøya (S), Sk, Skytttelodden. (C) Spitsbergen locations (Fairchild et al., 2016a, 2016b; Fairchild & Hambrey, 1984; Halverson et al., 2004; Harland et al., 1993). O, Ormen-Slangen; P, Pinnsvinryggen [officially unnamed nunatak at N78°43.1′, E18°09.8′]; G, Golitsyfjellet; K, Klofjellet; A, Andromedafjellet; Di, Ditlovtoppen; D, Dracoisen.

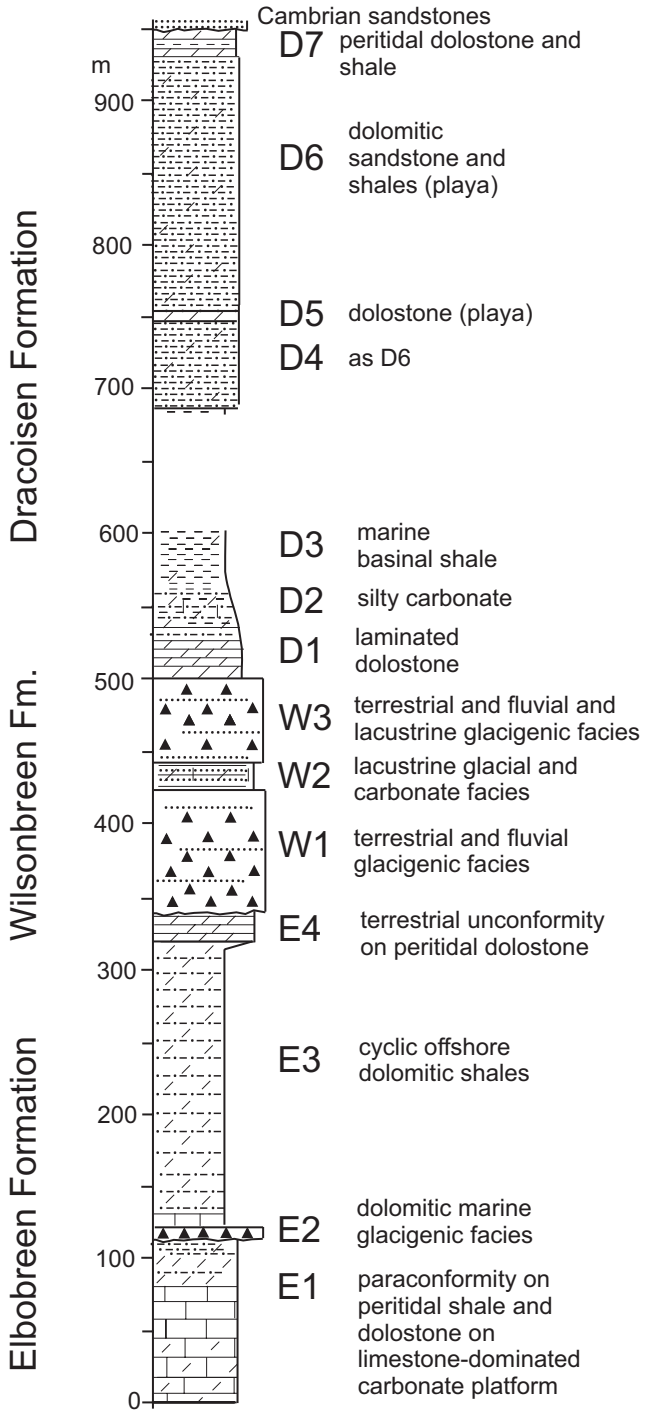

FIGURE 2 Summary stratigraphy of the late Tonian to mid-Ediacaran Polarisbreen Group with Members E1-E4 (Elbobreen Formation), W1-W3 (Wilsonbreen Formation) and D1-D7 (Dracoisen Formation) after Fairchild and Hambrey (1984). The Sturtian and Marinoan glaciations correspond, respectively, to Member E2 (Petrovbreen Member) and the Wilsonbreen Formation, both of which have disconformities corresponding to subaerial erosion at their base.

had previously been made on the basis of Sr and C isotope chemostratigraphy coupled with the sharply stratigraphically resolved evidence for glaciation (Chen et al., 2022; Halverson et al., 2020). Each glacigenic unit is overlain by a cap carbonate and the two caps show distinctly different lithologies and carbon isotope trends that compare respectively with the Sturtian and Marinoan caps as seen worldwide (Fairchild et al., 2016a; Halverson et al., 2004; Hoffman et al., 2012; Kennedy et al., 1998; Xiao & Narbonne, 2020).

The lower glacigenic unit, the Petrovbreen Member (E2) of the Elbobreen Formation (Figure 2), is predominantly glaciomarine. It displays interstratified limestone and glacigenic sediments near its top and is succeeded by a thin limestone interpreted as an offshore deposit, typical for a Sturtian cap (Fairchild et al., 2016a). The upper glacigenic unit, the Wilsonbreen Formation (Figure 2), is non-marine (Benn et al., 2015; Fairchild et al., 2016b; Fleming et al., 2016), and is overlain by a cap dolostone which is the subject of this paper (Figure 3). This is correlated with the Marinoan cap carbonate, the lower boundary of which was used to define the base of the Ediacaran System in South Australia (Knoll et al., 2006). In Svalbard (Figures 2 and 3), the cap is the lowest member of the Dracoisen Formation (D1) and grades through impure carbonates (D2) to black shale (D3) in a transgressive succession (Fairchild & Hambrey, 1984; Halverson et al., 2004). Millikin et al. (2022) report a Re–Os age of 631.2 ± 3.8 Ma from within D3 at a position 104 m above the base of the Dracoisen Formation in northern Ny Friesland, which fits well with the established 635 Ma age of the base of the Marinoan cap on different palaeocontinents.

In terms of basinal sedimentation patterns, it is notable that the pure carbonate shelf facies of the Tonian (up to the lower part of E1) are replaced by a dominance of dolomitic shale facies with dolomitic peritidal deposits for the later part of the Neoproterozoic succession. This is interrupted twice by panglaciation and once more by playa lake sediments (Members D4–D6) only to return in Member D7. Combined with evidence of aridity at numerous stratigraphic levels, the depositional basin has a distinctive character for over 100 Myr.

The shale domination in the Polarisbreen Group has been utilised to derive insights into oxygenation that have global relevance. Neoproterozoic oceans are thought, for the most part, to have been oxygen-deficient and rich in ferrous iron. The term 'ferruginous' (Canfield et al., 2007) has become standard for such an ocean (Swanner et al., 2020), despite a prior and more general usage for ferric environments. Tahata et al. (2015) carried out Fe isotope analysis on pyrite in shale from the Polarisbreen Group using laser-ablation inductively coupled plasma spectrometry. The $\delta^{56/54}$Fe values were positive before and after the Sturtian glacial (Member E2) pointing to ferruginous (rather than

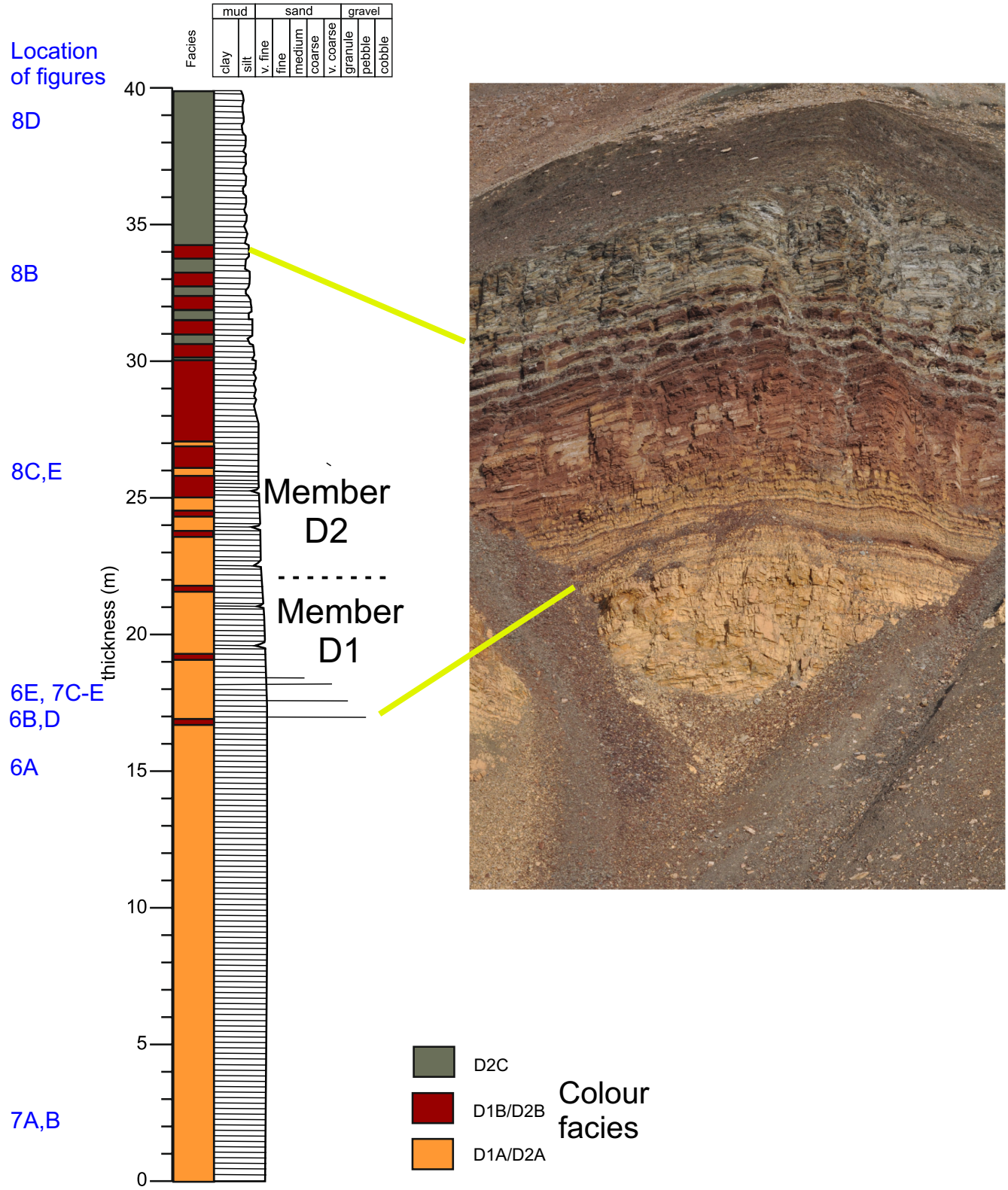

FIGURE 3 Log and photograph of Members D1 and D2, Ditlovtoppen. D1 is characterised by decreasingly pure dolostones transitioning upwards to D2 dolostone (and locally limestone) with quartz silt laminae, with increasing clay upwards. The top of the section is close to the base of Member 3 which is seen along section to the west, but here the section is truncated upwards by an unconformity with Carboniferous strata. The colour facies reflect the dominant iron minerals. The interbedding of red and green facies is interpreted to correspond with a precessional sedimentation rhythm.

oxic or euxinic/sulphidic) conditions, but sparse data from the Dracoisen Formation was more equivocal. Kunzmann et al. (2015, 2017a) carried out, respectively, iron speciation and bulk rock iron isotope analyses on the Polarisbreen Group including Members D2 and D3. Iron speciation data of the Dracoisen Formation revealed a pattern of suboxic to anoxic ferruginous conditions, comparable to pre-Marinoan samples. The Svalbard data, like those from North-West Canada, point to a lack of Mo-enrichment that characterises a strong oxygenation event found in South China (Sahoo et al., 2012). Kunzmann et al. (2015) attributed this to high organic matter loading associated with high productivity in the water column in the Svalbard (and equivalent Greenland) samples, but a more recent review suggests Mo-enrichment should only be present in euxinic facies (Algeo & Liu, 2020). Average slightly positive $\delta^{56/54}$Fe values in all post-Sturtian shales was interpreted qualitatively as due to oxidation of a larger proportion of ferrous iron in seawater and hence likely an increase in oxygenation compared with the pre-Sturtian. Sulphur isotope systematics (Kunzmann et al., 2017b), however, do record a signal of post-Marinoan increased oxygenation. Specifically, there is a parallel increase in δ^{33}S and δ^{34}S in Members D2 and D3 pointing to the establishment of the mechanism of bacterial sulphur disproportionation during re-oxidation associated with an increase of oxygen availability, but only after the Marinoan glaciation.

The post-depositional context is that Neoproterozoic strata in North-East Spitsbergen were buried under at least a few hundred metres of lower Palaeozoic sediment and subject to large-scale folding, local cleavage development, and later intrusion by plutons in the mid-Palaeozoic Ny Friesland orogeny (Harland et al., 1992). Burial temperatures of Cryogenian rocks in the study area did not exceed 160°C, based on incomplete solid-state ordering of clumped carbonate isotopes in calcites from Dracoisen (Mackey et al., 2020). Previous authors have argued that carbon isotope values in North-East Svalbard reflect values established during early diagenesis (Fairchild et al., 2016a, 2016b; Halverson et al., 2004). A lack of δ^{13}C-δ^{18}O covariation at any stratigraphic level indicates there is no prima facie argument for any meteoric or burial alteration to δ^{13}C. Carbonate platform sediments deeper in the pile also show no evidence of burial resetting of δ^{13}C (Halverson et al., 2018). The preservation of negative $\Delta^{17}O_{SO4}$ signals in CAS of syn-glacial limestones of the Wilsonbreen Formation, but not in coeval dolostones, was attributed to redox cycling of sulphate in evaporated water bodies in the case of the dolostones, rather than burial alteration (Bao et al., 2009; Benn et al., 2015). This interpretation is supported by the new data presented later.

3 | METHODS

Fieldwork in Olav V Land and Ny Friesland was carried out in 1982, 2010 and 2011 as part of a wider study of the Polarisbreen Group. Twenty samples of the cap carbonate were studied petrographically, including cold-cathode cathodoluminescence using 15 kV excitation (Fairchild et al., 2016a). Published carbonate carbon and oxygen isotope measurements were supplemented by 32 new analyses using standard techniques as detailed in Fairchild et al. (2016a). Carbonate-associated sulphate was also extracted from 14 samples for analysis of sulphate, δ^{18}O, Δ^{17}O and δ^{34}S values using methods documented in Benn et al. (2015). The parameter Δ^{17}O is defined as: $\Delta^{17}O = \ln(\delta^{17}O + 1) - 0.52 \times \ln(\delta^{18}O + 1)$. Negative values represent ^{17}O-depletion with respect to the reference line. The standard deviation associated with the Δ^{17}O is ±0.03% for multiple ($N < 3$) runs of the same O_2 gas on the MAT 253 mass spectrometer, and ±0.05% for replicates of the same $BaSO_4$ via laser-fluorination (Bao et al., 2008). Carbonate carbon and oxygen isotope results are presented in parts per thousand with respect to the Vienna-Pee Dee Belemnite (V-PDB) and sulphur isotopes relative to Canyon Diablo Troilite (CDT) using the conventional notation. Minor element analysis on the carbonate fraction (dilute nitric acid dissolution) was carried out by ICP-MS as described in Fairchild et al. (2016a). Geochemical data are presented in Table S1.

4 | SEDIMENTOLOGY OF THE POST-GLACIAL TRANSGRESSION (MEMBERS D1 AND D2)

Post-Marinoan successions are acknowledged to be one of the major marine transgressions in the stratigraphic record, with 600 m sea-level rise estimated from shallow-to-deep profiles at the Otavi/Swakop platform margin of Namibia (Hoffman et al., 2021). However, in North-East Svalbard, the deposits represent a section approximately parallel to depositional strike so that the sea-level rise following deposition of terrestrial and lacustrine glacigenic deposits of the underlying Wilsonbreen Formation and before deposition of the basal Ediacaran sediments, is unconstrained.

4.1 | Basal clastic sediments

The base of Member D1 is sharp, but only rarely exposed. At Dracoisen and Andromedafjellet, there is a thin tectonised clay gouge (exposed by trenching at the former) at the contact between dolostone above and diamictite below. In

contrast, Harland et al. (1993) noted the presence of a channelled top over diamictite at some Olav V Land locations and Tahata et al. (2015) noted the presence of a weathered, 1 m clastic interval at Sveanor, Nordaustlandet. The most informative example of the Olav V Land locations observed in this study is in the near-vertical strata at Pinnsvinryggen (Figure 4). Here, diamictite with thin sand-filled wedges several metres deep and a few centimetres wide (Figure 4A) is overlain by a 0.3 m thick horizontally stratified pebbly sandstone (Figure 4B) with polymict variably rounded terrigenous clasts (Figure 4C) and with well-rounded quartzofeldspathic coarse sand matrix (Figure 4D). In turn this is sharply overlain by dolostone (Figure 4A).

Benn et al. (2015) have interpreted the wedge structures in this Wilsonbreen section as periglacial in origin, consistent with overall interpretation of the Wilsonbreen as forming in a terrestrial glacial landscape that is flooded by the start of Dracoisen Formation deposition. A similar relationship of cap dolostone to periglacial structures is found in West Africa (Deynoux, 1982; Shields, 2005). Initial rounding of quartz grains in the thin intervening sandstone may have resulted from aeolian activity during glaciation (Fairchild et al., 2016b). The pebbly sandstone could be interpreted here as a beach deposit, consistent with evidence of wave action higher in D1, although a fluvial origin is also possible. Any surf zone reworking would anyway likely be brief during a rapid transgression.

4.2 | Member D1: laminated dolostone

4.2.1 | Facies, petrography and elemental geochemistry

Member D1 dolostone is similar throughout North-East Svalbard: millimetre-scale laminated and finely

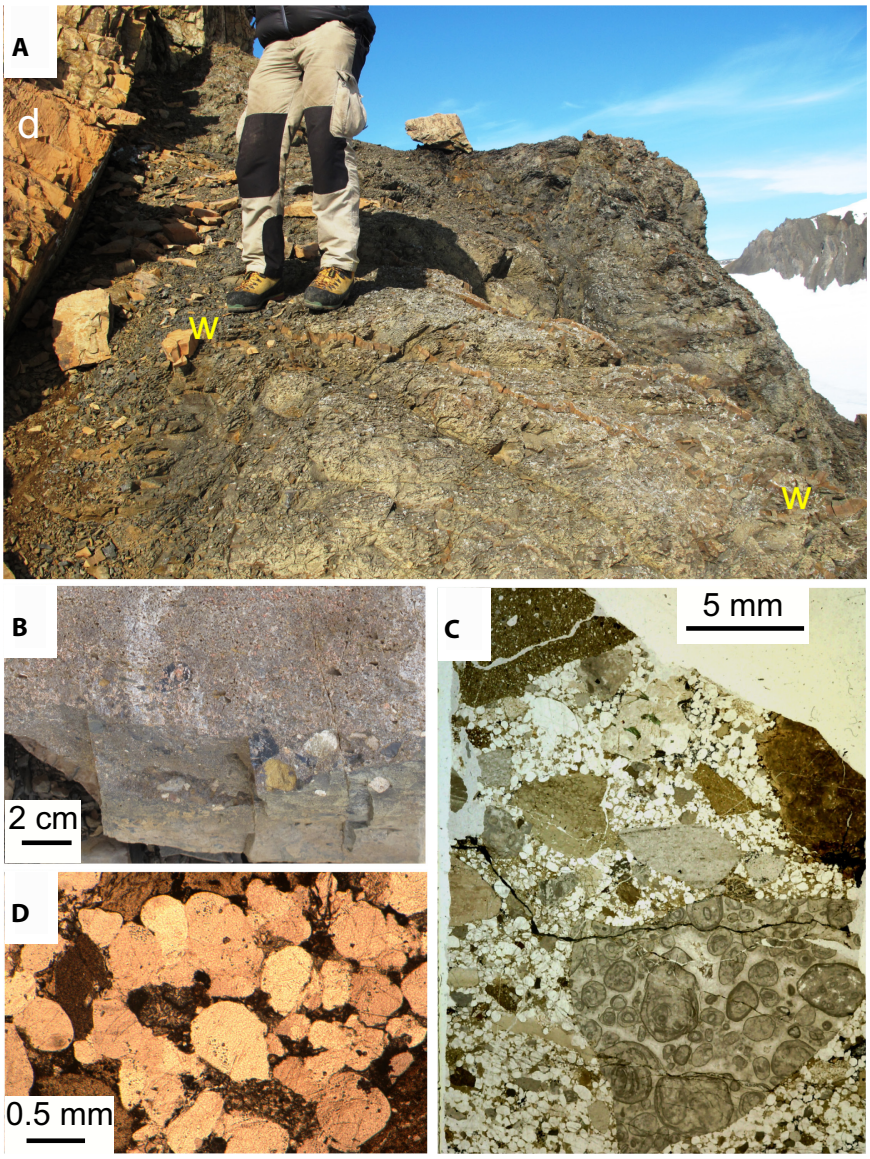

FIGURE 4 Pinnsvinryggen section. (A) Steeply dipping Dracoisen Formation dolostones resting on Wilsonbreen Formation diamictite; width of view 2 m. Letter 'd' indicates the dolostone. Letters w—w lie along a sandstone dyke interpreted as periglacial in origin. (B) Loose block of topmost Wilsonbreen Formation diamictite overlain by pebbly, stratified coarse-grained sandstone. (C) Thin section viewed in transmitted light of pebbly coarse-grained sandstone at Wilsonbreen–Dracoisen Formations' contact. Small pebbles include diamictite matrix (top) and pisolitic dolostone (lower right). (D) Photomicrograph in plane polarised light of sandstone thin section as in (C) illustrating rock fragments and well-rounded quartz grains.

crystalline. The main lateral change is a reduction in thickness of the cap dolostone (Member D1) in Nordaustlandet compared with adjoining North-East Spitsbergen. In Nordaustlandet, five sections exhibit a thickness of about 5 m (Edwards, 1976; Halverson et al., 2004), with a higher value of 10 m at Søre Russøya, although Tahata et al. (2015) recorded 20 m at Sveanor. In Spitsbergen, thicknesses range from 11 to 36 m with the thinnest values both to the north (Dracoisen 11 m, Halverson et al., 2004) and south (Golitsynfjellet,12 m Harland et al., 1993). In North-East Greenland, the cap dolostone disappears altogether to the south over 120 km distance (Hambrey & Spencer, 1987).

D1 is dominated by uniform, yellow-brown weathering dolostone with parallel or slightly undulatory lamination. However, the dominant feature is an indistinctly clotted structure on a scale of around 0.1 mm (corresponding to micropeloids of James et al., 2001), which would be consistent either with carbonate cementation or obliteration of transported peloids by minor compaction and crystal growth. This ambiguity applies particularly in the lower 10 m, where terrigenous debris is practically absent. Alternating laminae partially and completely cemented in early diagenesis are common and locally there are structures incompatible with simple mechanical layering. For example, Figure 5 illustrates millimetre-scale

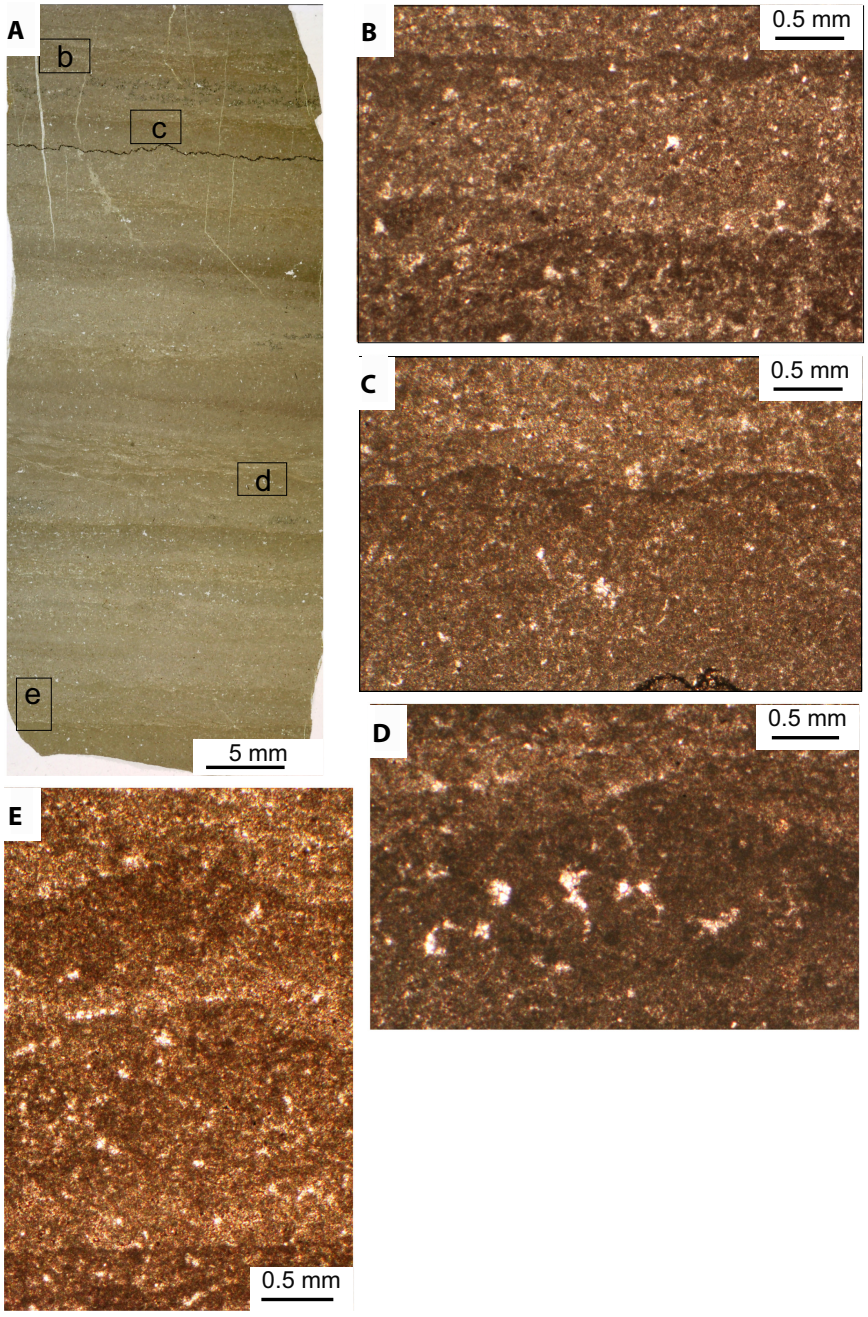

FIGURE 5 Petrographic microbial features in a sample 7 m above base of D1 at Andromedafjellet. (A) Whole thin section (width of view 20 mm) of laminated dolostone seen in transmitted light. Location of photomicrographs (B) to (E) are indicated by rectangles (each rectangle has a long axis of 3.63 mm). There is a small stylolite just below box c. (B) Dark, microbially cemented horizons with slightly mounded tops in peloidal dolostone. (C) Microbially cemented micro-mounds. (D) Micro-mound of dark micrite with internal dolomite-cemented fenestrae. (E) Three dark microbially cemented horizons, the upper one displaying mounded micro-relief.

layering (Figure 5A) in which a clotted fabric is present throughout, but where laminae are capped by a denser fabric (Figure 5B) which can display sub-millimetre-scale domes (Figure 5C,D,E) with fenestrae (Figure 5D,E). Such complex fabrics, although subtle, can be confidently identified as microbial, with carbonate precipitation focussed in extracellular polymeric substance (Dupraz et al., 2009; James et al., 2001).

Obvious clastic textures are less commonly seen in the Spitsbergen sections, but are clearly visible in the 15–20 m interval of the Ditlovtoppen section and locally at the base of the Pinnsvinryggen section. Here, petrographically, peloids are sometimes distinct, 50–100 μm in size and associated with 20–80 μm quartz silt (Figure 6A) and so are clearly transported grains. The detrital nature of the carbonate is clearly indicated by local distinct decimetre-scale fining-upwards beds with scoured bases and undulatory lamination (Figure 6B through E). These structures are indicative of combined-flows during storms. In the most easterly section at Aldousbreen (Edwards, 1976), distinct sandy turbidite beds occur, implying a deeper setting there. Elsewhere in Nordaustlandet, more spectacular features are reported: large-scale wave ripples persisting

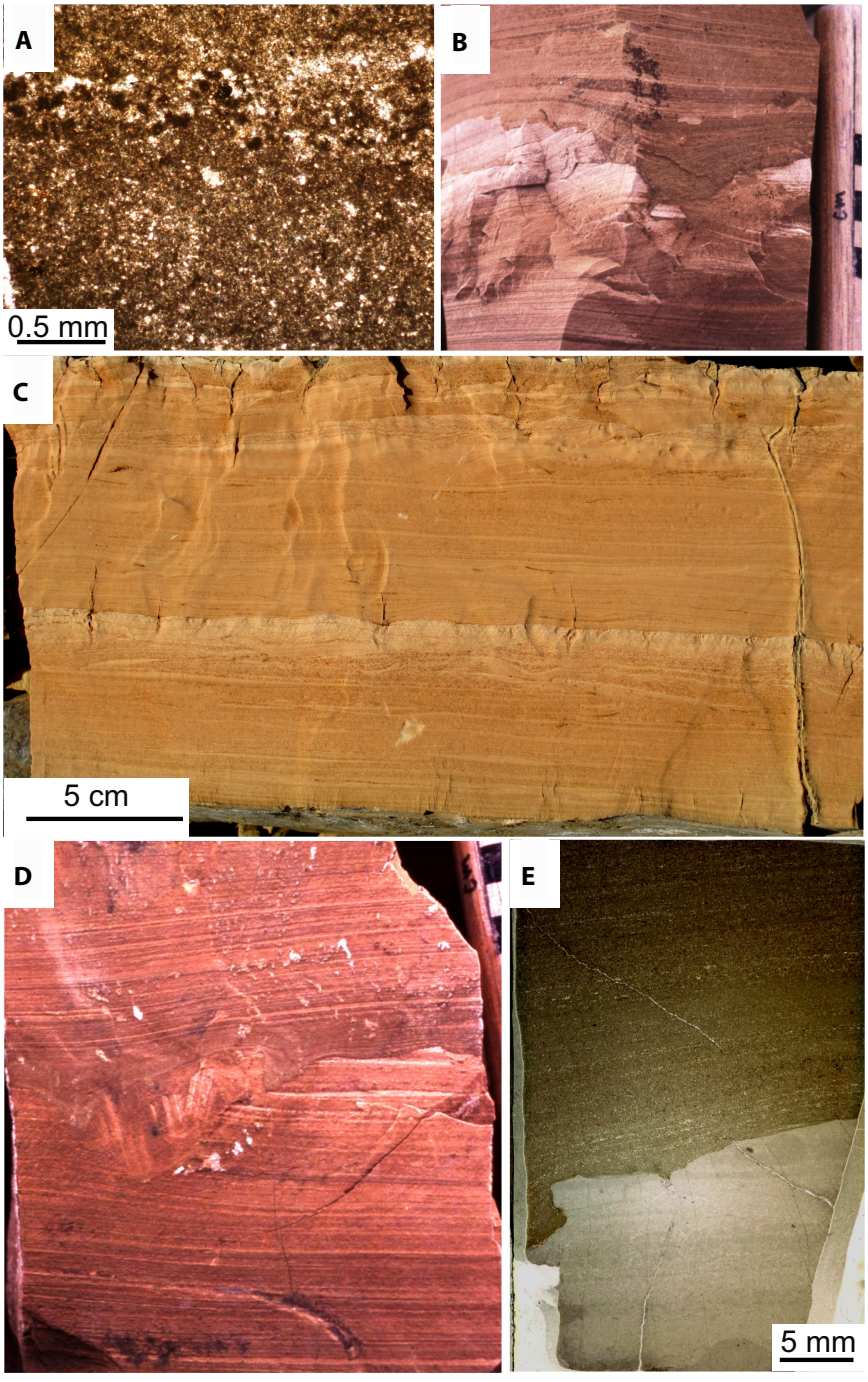

FIGURE 6 Clastic and erosional structures, Member D1 at Ditlovtoppen (A,B, D,E) and Pinnsvinryggen (C). (A) Dolostone with clotted texture and conspicuous layer with quartz silt and dark peloids near top. (B) Undulatory laminated silty dolostone fining-upwards to pure dolomite (centre) with irregular erosion surface. (C) Pinnsvinryggen, upper part of D1. Dolostone with undulose lamination arranged in two, probable storm-generated packages with purer finer dolomite top. (D) Undulatory laminae in dolostone, centimetre-scale at top right. Depression in irregular erosion surface is occupied by cemented laminated dolostone clasts. (E) Whole thin section, transmitted light. impure peloidal and silty dolostone overlying erosion surface on pure peloidal dolostone.

upwards for up to 1.5 m in the upper half of the cap (Allen & Hoffman, 2005; Halverson et al., 2004). These were originally interpreted as evincing non-actualistic storm waves, more powerful than in the Phanerozoic, although Lamb et al. (2012) showed that wave conditions were within limits of modern storms. From similar examples in South Australia, Rose and Maloof (2010) pointed out that such phenomena would cause rapid and deep mixing of the water column.

At the Ditlovtoppen section, the tops of storm beds are clearly cemented prior to erosion (Figure 6B) and production of intraclasts (Figure 6D) and a similar observation was made of edgewise dolostone breccias at Aldousbreen (Edwards, 1976). A key observation in the current study is the sharp upper boundary of pure dolostone layers overlain by silty dolostone detritus indicating that they were hardgrounds (Figure 6E). The cementation process evidently is the formation of mosaics of finely crystalline dolomite (10–30 μm). Some exposures, notably at Ditlovtoppen, display alternating dark and light laminae where the light laminae were completely cemented by dolomite in early diagenesis whereas the dark laminae contain bitumen, a relic of hydrocarbon that had filled residual porosity.

Crystals display red cathodoluminescence (CL, Figure 7). The CL zonation is common to all crystals on the thin section scale (Figure 7B) in this case with a moderate-bright zone, followed by a brighter zone

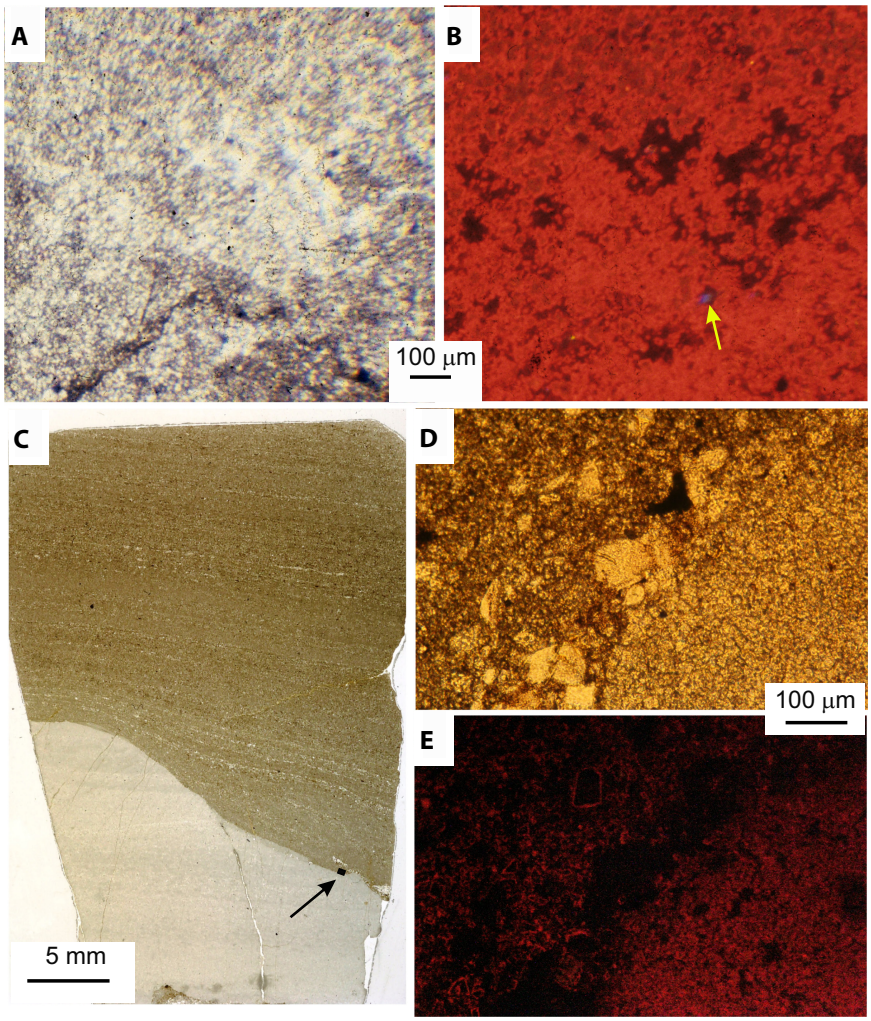

FIGURE 7 Ditlovtoppen section. (A and B) Transmitted light and cathodoluminescence (CL) images of dolomite, 2 m above base of D1. Complex peloidal fabric with dark stylolite. In the CL image, dolomite crystals (10–20 μm) show consistent zonation with earliest (moderately bright) zones more conspicuous at top of field followed by bright red dolomite whilst late growth into small fenestrae is dark. Small blue K-feldspar grain is arrowed. (C) Whole thin section, transmitted light. Impure peloidal and silty dolostone overlying erosion surface on pure peloidal dolostone. Arrowed black rectangle is location of (D) and (E). (D) Transmitted light and (E) CL image across the erosion surface. Lower right area is below the erosion surface and exhibits predominantly moderate-bright CL. Upper left area is above the erosion surface, crystals displaying no CL in early growth then a bright zone, then dull CL. Dolomite crystals above and below the erosion surface evidently formed at different times, consistent with syn-depositional dolomitisation.

and then duller CL for later growth into small fenestrae (Figure 7B). A similar pattern of CL zonation is seen in dolomite cement fans in the Nucculeena cap carbonate of South Australia (Hood & Wallace, 2018). As in that example, the preservation of CL zonation in dolomite crystals in D1 points to an absence of dissolution-precipitation processes and hence a preservation of primary chemistry in crystal interiors. In detail, the CL zonation differs at different horizons and Figure 7C,D,E illustrates a change in the CL zonation pattern below and above a hardground erosion surface. This indicates the dolomite crystals grew at different times and implies that the bulk of the overlying carbonate within the area of Figure 7D,E was $CaCO_3$ at the time of deposition, notwithstanding the presence of intraclastic dolomite within the storm sediments in general.

New minor element data in dolomite soluble in dilute acid (Table S1) are very similar to those presented by Halverson et al. (2004) and Tahata et al. (2015). Combining the data sets, the ranges are 40–74 ppm Sr, 400–5000 ppm Mn, 5000–13 000 ppm Fe and 1200–3800 ppm Na. In D1, pyrite is only present in trace quantities and Tahata et al. (2015) found it to be cubic rather than framboidal. Trace species Fe and Mn show an irregular variation with stratigraphic height, but Sr shows a fairly consistent increase from 55 to 75 ppm (Table S1) upwards. Sulphate concentrations (mean 603 ppm) are discussed later. The $^{87}Sr/^{86}Sr$ ratios on the D1 cap determined by Tahata et al. (2015) are mostly between 0.710 and 0.711, with one sample at 0.7086. These are rather greater than the lowest marine values found elsewhere (0.7072, Chen et al., 2022). The addition of some radiogenic ^{87}Sr post-depositionally is normal for Neoproterozoic dolostones and especially given the low Sr content of D1 dolomite.

4.2.2 | Interpretation: initial $CaCO_3$ deposition

The above observations and comparators reinforce an early conclusion that dolomitisation in D1 is replacive, presumably of calcium carbonate (Fairchild & Spiro, 1987). Shields (2005) postulated that much of the original carbonate in cap dolostones was precipitated as microcrystalline inorganic whitings from a proposed freshwater lid, highly supersaturated for $CaCO_3$. This precipitation was inferred to be triggered by photosynthetic activity. Considering that precipitation is more efficient in low ionic strength solutions, photosynthetic activity would be a viable trigger for calcium carbonate precipitation regardless of the water salinity.

Given the evidence for storm action on the D1 shelf, this calcareous material would have accumulated offshore and so there may have been minimal sedimentation close to the shoreline. At a critical water depth, net sediment accumulation occurred, and dolomite formation led to lithification where sediment was sufficiently undisturbed. There is clear evidence for microbial binding of this sediment in the lower half of D1 and the generation of micropeloidal clotted structures in otherwise uncemented sediments, although it is uncertain whether these clots were originally $CaCO_3$ or dolomite.

More direct evidence of a freshwater role in the genesis of D1 may be the presence of the ^{17}O-anomalous CAS described in Section 3.3.1. This anomaly must have been generated by oxidation of sulphides to sulphate in contact with molecular oxygen in a CO_2-rich atmosphere (Bao et al., 2008, 2009; Benn et al., 2015). This distinctive sulphate can be generated in a continental setting and transferred in non-marine waters to the sea. There it co-precipitated with carbonate phases.

4.2.3 | Interpretation: dolomitisation

The theoretical generation of a kilometre-thick column of freshwater on deglaciation (Shields, 2005) has led to a supposition that 'cap dolostones formed predominantly in a freshwater environment' (Yang et al., 2017). This begs the age-old question of the Mg-source, since freshwaters generally today, and at the end of Marinoan glaciation on the adjoining continent to the D1 sections, had Mg/Ca ratios much less than one (Fairchild et al., 2016b). Hence ikaite and calcite were the initial precipitates in the Marinoan glacial lakes, except where modified by evaporation (Fairchild et al., 2016b). Thus, in the absence of evidence for evaporation, dolomitisation of D1 requires marine-dominant solutions.

Ahm et al. (2019) examined the potential role of dolomitisation by geothermal marine pore water convection using a numerical model. This model is led by the observation of coupled changes in Ca and Mg isotopes and unexplained lateral variations in $\delta^{13}C$ (Ahm et al., 2019; Hoffman & Lamothe, 2019) and was developed from the approach of Higgins et al. (2018) contrasting the behaviour of fluid-buffered and sediment-buffered diagenetic systems. The Neoproterozoic case was a reapplication of such an approach designed to explain modern aragonite to calcite neomorphism and dolomite cementation on the Bahamian platform (Ahm et al., 2018), but obtains the curious result when applied to the cap carbonates that the molar Mg/Ca ratios of the dolomitising fluid is only 0.9. In contrast, the Svalbard cap rests on a ramp, not a platform, and the syngenicity and complete and rapid

dolomitisation argue for a more aggressively dolomitising marine water.

Interpretation of D1 in contrast stems primarily from the petrological observations. In D1, where carbonate sediment remained undisturbed for long enough, lithification by dolomite occurred very close to the sediment surface, with intraclasts ranging from micropeloids to decimetre scale in size. Therefore, on sedimentological grounds, D1 compares with the firmground/hardground dolostone horizons described at four stratigraphic levels in the Cryogenian to Ediacaran succession of South Australia by Wallace et al. (2019) and compared to cap carbonates. The key ingredients are sediment starvation and anoxic marine water chemistry favourable to dolomite precipitation. The Australian examples are more varied in carbon isotope signatures, however, as well as displaying evidence of displacive growth as seen commonly in other caps where brecciation associated with isopachous mineral growths is found (Shields, 2005). The Svalbard dolomite crystals grew more passively, presumably reflecting lower supersaturation, but the occurrence as lithified horizons exhumed by storm action is a powerful point of comparison. Murray et al. (2021) demonstrated that hardgrounds on the margin of the modern Great Bahama Bank were associated with fluid-dominated diagenesis in which CAS in dolomites had seawater isotopic signatures. If this applies also to the D1 hardgrounds, it would imply that the dolomite does not inherit chemical characteristics of the primary $CaCO_3$ precipitate. Hence, the upward moderate increase in Sr concentration within D1 is a signal of changing chemistry of the seawater-dominated depositional water, with reducing freshwater influence.

Hood and Wallace (2018) noted the Neoproterozoic Era as a time period where aragonite, Mg-calcite and dolomite marine mineralogy is favoured for which they identified high solution Mg/Ca ratios as the simplest and most obvious driver. Interactions of silicates with anoxic ferruginous seawater would favour more net Mg release to solution than in oxic Phanerozoic waters (Wallmann et al., 2008). Another factor is inferred high alkalinity promoted by microbially catalysed reduction reactions (Higgins et al., 2009). Low sulphate concentrations are known to favour dolomite formation, but whereas petrographic evidence for dolomite formation coincident with sulphate reduction to form sulphides is present in some Neoproterozoic carbonates (Hood & Wallace, 2015; Hu et al., 2020; Shuster et al., 2018), such is absent in D1 where dolomite contains significant sulphate and pyrite is rare. Another catalyst for dolomite formation that is relevant to D1 is the extracellular polymeric substance (EPS) of microbial mats. The physical biogeochemistry that favours Mg-rich carbonate precipitation in such matrices was discussed in detail by Petrash et al. (2017). Disordered dolomite formation in EPS has been demonstrated experimentally in a model anoxic seawater (Krause et al., 2012) and, in the presence of Mn^{2+} Daye et al. (2019) demonstrated the growth of dolomite with ordering reflections. In D1 sediments with a clotted fabric, the dolomite may not have simply replaced calcium carbonate but may, to some degree, have grown as primary precipitates within a solid matrix of EPS secreted by cyanobacteria.

4.2.4 | Interpretation: redox reactions

A key problem in interpreting carbonate geochemistry is to distinguish signals of the depositional water from those imposed by diagenesis. Variations in CL within crystals can be used to infer that Mn and Fe variability are imposed by early diagenesis. Although CL can be activated by rare-earth elements, particularly using the sensitive hot-cathode technique, cold-cathode-stimulated CL can normally be attributed to activation by Mn^{2+} and quenching by Fe^{2+} (Fairchild, 1983; Richter et al., 2003). Hood and Wallace (2015) noted that the preservation of primary cathodoluminescent growth zonation indicates no mobility of Fe or Mn during subsequent diagenesis. Here Hood and Wallace (2015) and Hu et al. (2020) are followed in relating temporally varying dolomite chemistry to understanding early diagenetic microbially catalysed reactions in which a succession of luminescent zones reflect falling Eh (Barnaby & Rimstdit, 1989). Such reactions ordered by free energy yield within decimetres of the sediment surface, leads to oxygen removal at depth followed by reduction of Mn-oxides to Mn^{2+}, Fe-oxides to Fe^{2+} and sulphate to sulphide (Algeo & Liu, 2020; Burdige, 1993). In practice, the crystallinity of the oxides varies, causing the Mn and Fe-reduction zones to overlap (Burdige, 1993). In the case of D1, the presence of CL zonation demonstrates temporally varying Fe-Mn chemistry in pore water and the predominance of moderately bright luminescence is consistent with its mean Fe-Mn chemistry (cf. Fairchild, 1983). This implies oxygen-free conditions were readily established in porewater with both Mn and Fe-reduction active, but sulphidic conditions were not reached. The Fe-Mn chemistry of the dolomite is consistent with the dominant suboxic to anoxic conditions in the Polarisbreen Group inferred in the iron speciation study of Kunzmann et al. (2015).

A wide variety of redox proxies have been trialled on cap carbonates (Jin et al., 2018; Sahoo et al., 2012). Whilst the results are mostly consistent with weakly anoxic conditions, many data fit with expected heterogeneity of water masses. A general conclusion is that a substantial increase in oxygenation is not encountered until later in the Ediacaran (Wallace et al., 2017).

4.2.5 | Interpretation: comparison with other cap successions

The basic lithology of D1 closely resembles many other Marinoan caps worldwide (Hoffman et al., 2007; James et al., 2001; Kennedy, 1996). There is evidence in regions with a wide range in palaeobathymetry that shallow water structures in the cap carbonate are present on the distal foreslope. Hence the carbonate is diachronous and deposition accompanied sea-level rise (Hoffman et al., 2007, 2017). Whilst some caps have similar lack of facies variation to D1-D2, most demonstrate greater variability in facies which Kuang et al. (2022) attribute to a further down-ramp setting, although there are also likely to be basin-specific factors. Some caps contain columnar stromatolites and can be overlain by limestone, locally with sea-floor aragonite fans and barite precipitates; some are cherty. The lack of barite in Svalbard is likely linked to an absence of deep upwelling waters (cf. Peng et al., 2011) which in turn reflects the shallow intracratonic basin of deposition. The paucity of siliciclastic detritus in most cap successions can be explained either in a model of very rapid deposition in an ocean grossly supersaturated for $CaCO_3$ (Hoffman et al., 2021) or by slow deposition on a shelf starved of sediment because of sediment trapping in estuaries (Nordsvan et al., 2019). In the discussion, a model for D1 is developed that accommodates both sedimentation rate perspectives (Penman & Rooney, 2019).

4.3 | Member D2: impure carbonates and rhythmicity

Member D2 consists of less pure carbonates than Member D1 and is also more characteristically red or green in colour (Figures 3 and 8A) reflecting iron in oxide or silicate phases as well as within the dolomite crystal lattice. Silt laminae are dominated by quartzo-feldspathic debris (30–50 μm, Figure 8B), whereas 20–30 μm siliciclastic debris is more typical of the dolomite laminae and clay is minor. Locally, there are centimetre-scale fining-upwards units with minor erosion at their base (Figure 8A,D). Calcite develops as a microsparry to sparry cement in coarser laminae and can largely replace pre-existing more finely crystalline dolomite (Figure 8C,E). This is a similar, probable shallow to deep burial paragenesis, as calcite in the shaley dolostones of Member E3 of the underlying mid-Cryogenian Elbobreen Formation (Fairchild et al., 2016a).

The lithology of D2 is consistent with continued deepening of the transgressive system, with the thinner units than Member D1 related to less carbonate sediment reaching deeper water whilst siliciclastic sediment would have a distinct fluvial source; thicker units of such sediment are seen in the easternmost Aldousbreen section in Nordaustlandet (Edwards, 1976).

The colour variation around the D1-D2 boundary includes a series of five distinct red-green alternations in 4.8 m of section at Ditlovtoppen (Figure 3). Differential weathering has occurred, with reddened bands being slightly more resistant and this pattern continues in the grey-green strata above (Figure 3). This implies that there is also a cyclicity in the carbonate/siliciclastic ratio and hence an underlying primary control on the banding. The colour variation appears to be superimposed later. Secondary reddening in the underlying Wilsonbreen Formation was demonstrated by small-scale Liesegang band structures and is consistent with the organic-poor nature of this formation (Fairchild & Hambrey, 1984). The colour-banding at the D1-D2 boundary was likewise originally interpreted as simply a burial diagenetic feature: a large-scale Liesegang band structure between the oxic Wilsonbreen Formation and anoxic Dracoisen Formation (Fairchild & Hambrey, 1984). The primary origin of the cycles at the D1–D2 boundary compares with a slightly thinner (0.5 m scale) precessional rhythm expressed as a subtle variation in sediment composition which dominates the underlying Member E3 of the Elbobreen Formation in the study area, with 200 visually obvious cycles developed (Fairchild et al., 2016a). Climate modelling suggests that precession also controlled glacial advances in the late Cryogenian Wilsonbreen Formation (Benn et al., 2015). Hence, a subtle precession-controlled variation in sediment composition is the favoured interpretation of these structures at the D1–D2 boundary. In the discussion, the constraint of a mean 0.95 m thickness of precessional cycles is input into the sedimentation model. Such cycles were estimated by Waltham (2015) to have a duration of 18 kyr at 600 Ma.

5 | CARBON ISOTOPE AND $\Delta^{17}O_{CAS}$ RELATIONSHIPS

5.1 | Carbon isotopes

The carbon isotope systematics of cap carbonates have been a major theme since the advent of Snowball Earth theory (Hoffman et al., 1998). It was originally thought that Marinoan caps are characterised by increasingly negative values with stratigraphic height (Halverson et al., 2005) and attempts made to interpret it as a primary signal that is correlatable worldwide, but no agreed mechanism emerged for the variation (Fairchild & Kennedy, 2007; Yu et al., 2020). Possibilities include the consequences of methane release, Rayleigh distillation of an initial CO_2-enriched atmosphere or significant temperature increase.

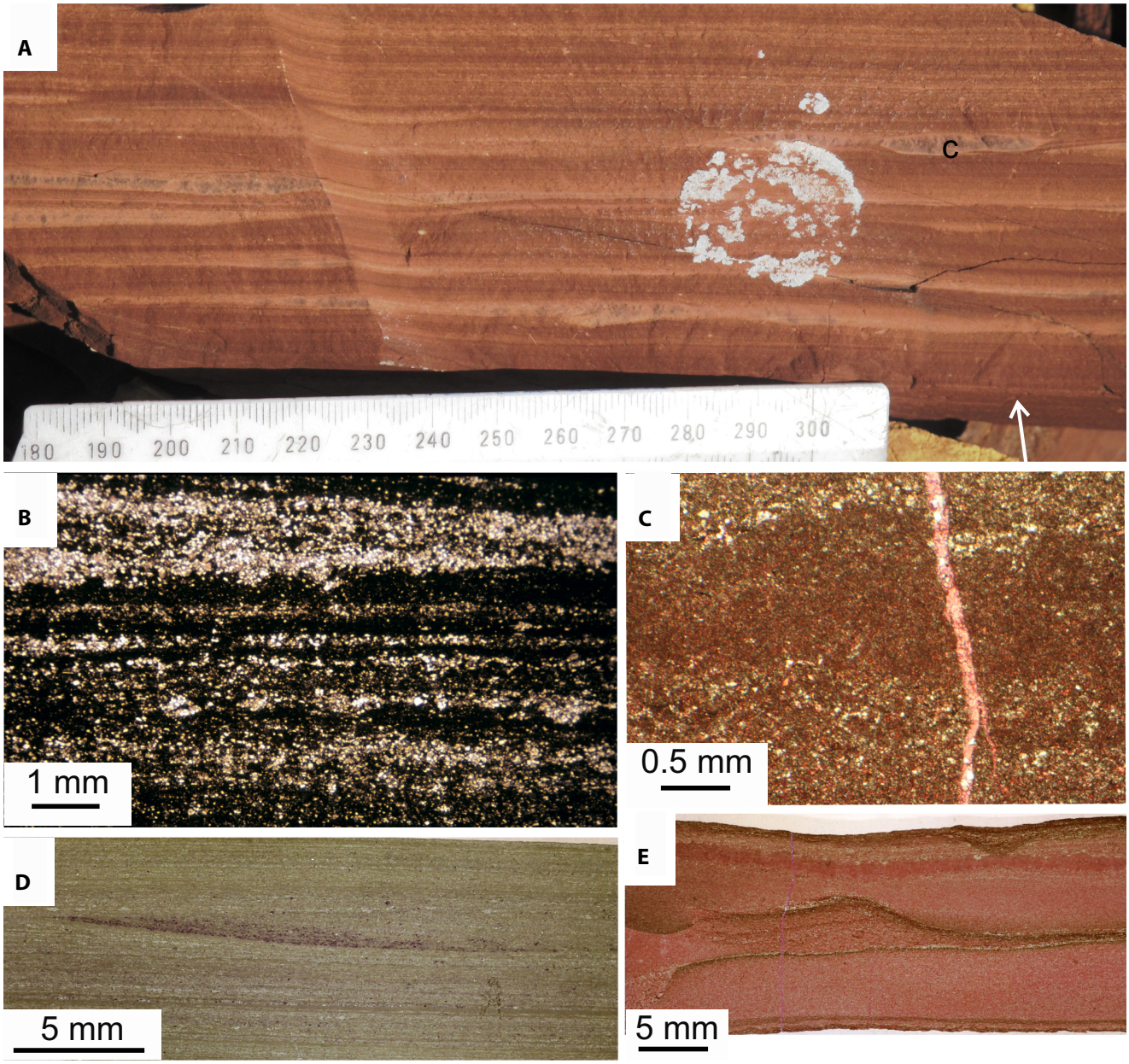

FIGURE 8 Member D2. Field photograph from Pinnsvinryggen (A) and thin sections from Ditlovtoppen (B–E) the latter having calcite stained red with Alizarin Red S. (A) Laminated silty pink (haematitic) dolostone with centimetre-scale units with slightly scoured bases, fining upward. Small concretion denoted by letter "c". Scale in mm and cm. Circular white area is a modern lichen. (B) Plane polarised light image (9 mm field of view) of laminated dolostone with laminae rich in quartz silt with calcite cement. (C) Photomicrograph in plane polarised light of laminated silty largely calcitised dolostone (calcite is stained pink with Alizarin Red S) cut by calcite vein. (D) Whole thin section in transmitted light of laminated silty dolostone with scour-surface marked by calcite cementation. (E) Whole thin section in transmitted light. Laminated microsparry limestone with small scour structures and relic dolostone (grey) areas.

Hoffman et al. (2007) demonstrated diachronous cap carbonate formation with a total $\delta^{13}C$ decline upwards of 4.4‰ across a 0.5 km palaeoslope in Namibia and only small (1‰) lateral variation. That study clearly indicates that the majority of preserved cap dolostone sections worldwide, in shelf settings, represent a stage in the post-glacial transgression when sea level had already risen some hundreds of metres. More recently, more comprehensive data compilations show that vertical variation in carbon isotopes can be irregular or non-existent (Lang et al., 2016).

In Svalbard, an upwards-declining stratigraphic trend in $\delta^{13}C$ values was demonstrated to be shared by multiple sections in Svalbard by Halverson et al. (2004) and Tahata et al. (2015). Figure 9A shows these results combined with the new data demonstrating a compact trend of decreasing $\delta^{13}C$ values with time, although there are a few outlying low points, most of which also have low

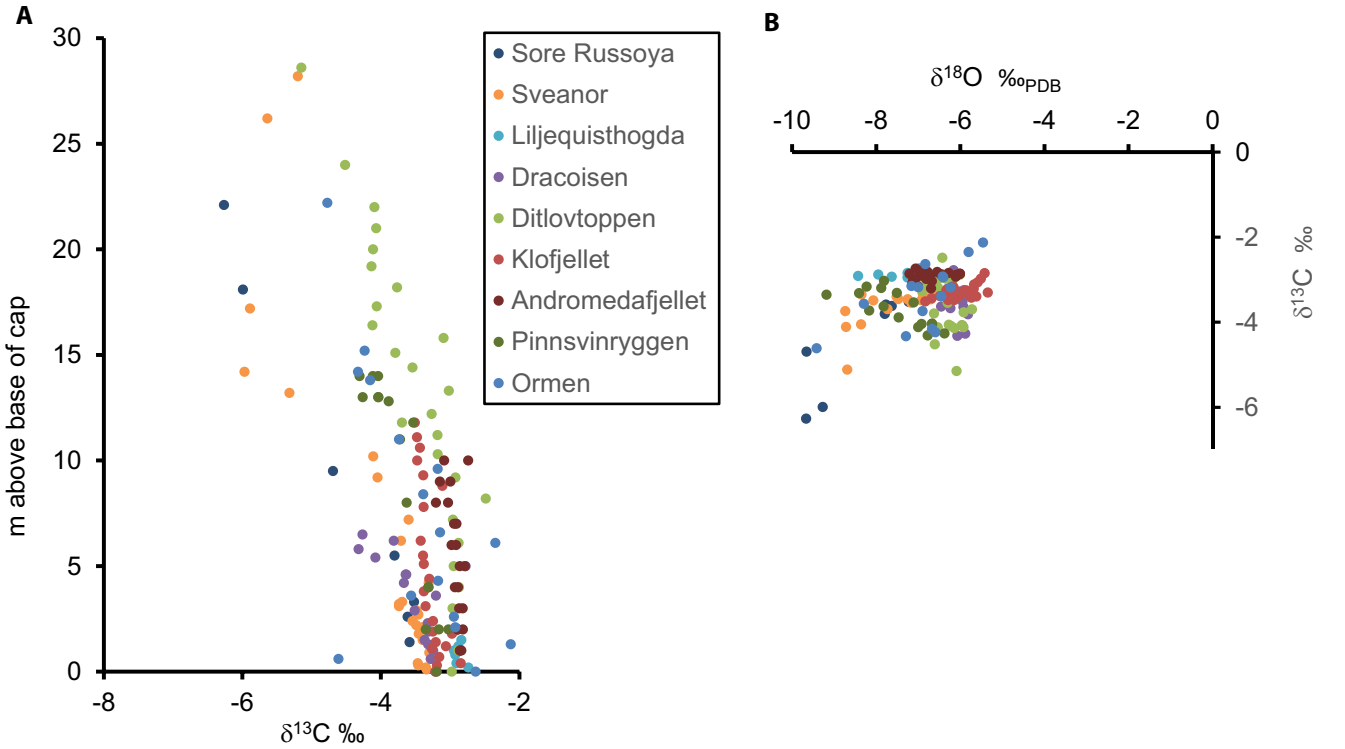

FIGURE 9 Geochemical data from Members D1–D2. **(A)** Plot of stratigraphic variation in carbon isotopes from Spitsbergen and Nordaustlandet sections (Halverson et al., 2004, Tahata et al., 2015 and herein). The key arranges the sections from north to south. There is a steady decline in $\delta^{13}C$ with height and minor differences between sections. (B) Cross-plot of oxygen and carbon isotopes of the data shown in (A). Data cluster with a few outlying low values in $\delta^{18}O$ that are mostly also outliers in $\delta^{13}C$.

$\delta^{18}O$ value (Figure 9B), implying that these are not primary values. The offset to lower values in the two most northerly sections (Søre Russøya and Sveanor, which are also thin) could be attributable to diachroneity of onset of carbonate sedimentation, with these sections being younger. Otherwise, the tight data trend is consistent with the signal being a primary one, with strong wave action helping to homogenise the water chemistry. It is likely that little change in $\delta^{13}C$ accompanied dolomitisation because of buffering by the pre-existing $CaCO_3$. Alkalinity generated from isotopically light organic carbon during Fe and Mn-reduction reactions in pore waters would have led to a depression in $\delta^{13}C$ values, but these metals are only minor components so the effect is small.

For the carbon isotope data as a whole, there is a key ambiguity in the conflation of time and water depth: younger horizons, deposited in deeper water, have lighter values. Whilst some favour a time-evolution control for such patterns (Hoffman et al., 2021), He et al. (2021), in a global compilation, demonstrated a clear offset between shallow and deep-water settings in terms of $\delta^{13}C$, attributing the lighter values of deeper settings as related to increased remobilisation of organic carbon in the water column. A persistent depth-stratification of carbon isotopes requires that the sedimentary basin has a large volume to area ratio (which is conceivable in the Svalbard case), because otherwise stratification would be destroyed by wind-induced mixing. In summary, the Svalbard data reflect a common, but not universal trend in cap dolostones towards lighter signatures during transgression.

5.2 | Carbonate-associated sulphate isotopes

The potential for mass-independent (or mass-anomalous) $^{17}O/^{16}O$ fractionation with respect to $^{18}O/^{16}O$ (Thiemens, 1983) to be used as an environmental proxy in deep time sulphates was demonstrated by Bao et al. (2008) and reviewed by Crockford et al. (2019a). Bao et al. (2008) posited that the mass-anomalous ^{17}O-depletion found in post-Marinoan barite globally reflected a high atmospheric PCO_2. Mass-independent fractionation in the stratosphere results in an enrichment in ^{17}O in ozone and carbon dioxide and a depletion in molecular oxygen, with the degree of depletion in O_2 becoming larger with increasing PCO_2. The oxygen mixes with the troposphere where the signal can be transferred to the sulphate molecule by oxidation of sulphides on the Earth's surface. This sulphate in turn can be preserved in the geological record as barite or as CAS. In the case of CAS, sulphate substitutes for the carbonate ion. This has been studied experimentally in calcite by

Wynn et al. (2018) and growth rate, pH (competition between sulphate and carbonate ions) and absolute sulphate concentration emerge as key controls. Similar sulphate concentrations characterise limestones and dolostones of the same depositional setting (Benn et al., 2015). In minerals, sulphate oxygen isotope composition remains intact over geological time if the post-depositional alteration has not been excessively high in temperature–time terms. The Svalbard rocks were subject to much less thermal alteration than rocks in the European Alps that displayed some diagenetic shifts in CAS oxygen isotopes by exchange with carbonate (Fichtner et al., 2017). Before being incorporated in minerals, sulphate oxygen isotope composition can be reset via microbial reduction and re-oxidation in solution.

For sulphates formed today via oxidative weathering, its $\Delta^{17}O$ is *ca* −0.10‰. Study of syn-glacial carbonates from the Wilsonbreen Formation of Spitsbergen (Bao et al., 2009) revealed $\Delta^{17}O_{CAS}$ values as negative as −1.64‰ covarying with $\delta^{34}S$ towards a ^{34}S-rich end-member that lacked a distinct ^{17}O anomaly. The unusual ^{17}O-depletion was interpreted as indicating an exceptionally high PCO_2 (Bao et al., 2009). Following further sampling, this was argued to persist at a similarly high level through several likely precessional cycles close to the end of the Marinoan ice age (Benn et al., 2015). Another process that influences the $\Delta^{17}O$ value is the O_2 flux from photosynthesis which generates O_2 with $\Delta^{17}O$ with a value of 0, so that the anomaly in atmospheric O_2 would be larger if there is little photosynthesis. Modelling by Cao and Bao (2013) indicates the CO_2 effect should dominate since many independent lines of evidence (e.g. Zn and Cd isotope data, John et al., 2017) support a vigorous primary productivity at the onset of deglaciation.

Presented here are new $\Delta^{17}O_{CAS}$ values from D1 demonstrating the presence of a post-glacial CAS anomaly changing from around −0.6‰ near the base of D1 to around −0.3‰, 14 m above the base (Figure 7F). A D2 sample at 38 m above the base of D1 had a value of −0.23‰, which is approaching the expected background value. The values and variation with height are similar to the only other reported find of ^{17}O anomalies in CAS (Figure 10C): the Moonlight Valley cap of Western Australia (Bao et al., 2012). No vertical trend in $\delta^{18}O_{CAS}$ is observed in either section (Figure 10A), whilst $\delta^{34}S_{CAS}$ increases slightly in the Australian example, but not in the Svalbard data (Figure 10B). The sulphate concentration calculated to be in the carbonate fraction of D1 dolostones averages 603 ppm with a range of 250–1100 ppm (Table S1) and shows no correlation with $\Delta^{17}O_{CAS}$. The CAS concentrations are much lower than the continental carbonates in the Wilsonbreen Formation (Benn et al., 2015), although higher than Neoproterozoic dolostones in general (Hurtgen et al., 2002). The data trends differ from barite ^{17}O from other locations and are interpreted below.

6 | DISCUSSION

6.1 | Cap carbonates in the snowball earth narrative

Snowball Earth theory is at the heart of a resurgent interest in Neoproterozoic Earth history. This theory has

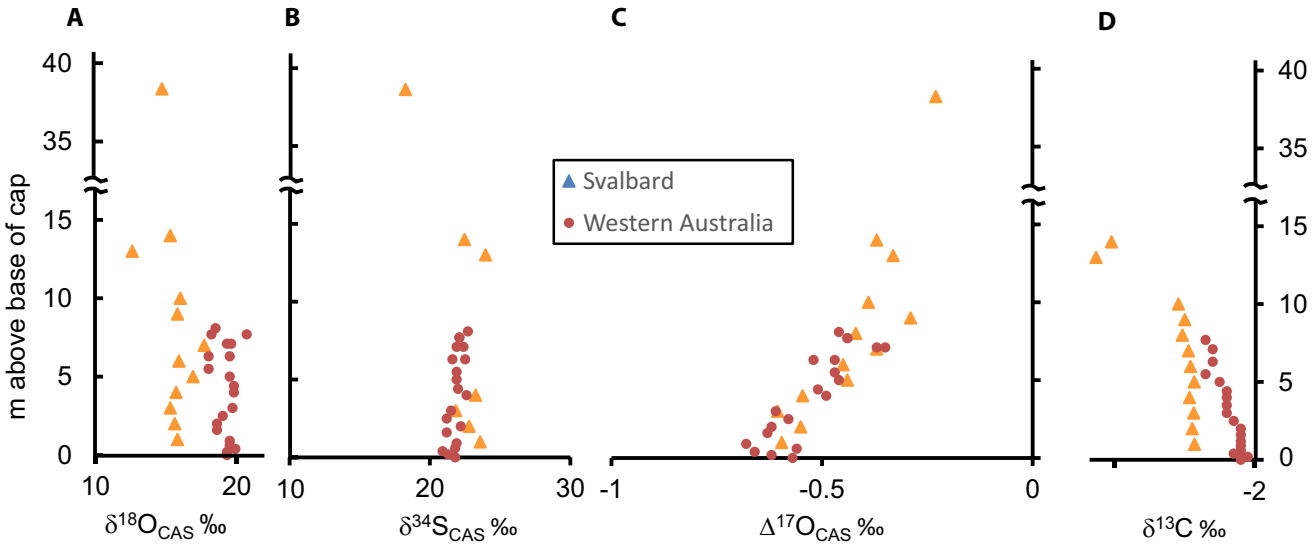

FIGURE 10 (A) Stratigraphic variation of $\delta^{18}O_{CAS}$. Variation is limited implying no sulphate is created by re-oxidation during deposition; Australian data is offset to higher values. (B) Stratigraphic variation in $\delta^{34}S_{CAS}$ showing a limited rise in the Australian data and no trend in the Svalbard data. (C) Stratigraphic variation in $\Delta^{17}O_{CAS}$ illustrating a significant decline in the negative anomaly with time. (D) Comparison of the Australian trend in $\delta^{13}C$ with stratigraphic height with that from Svalbard (the latter is a sub-set of Figure 9A).

evolved in response to new field data and model simulations (Hoffman et al., 2017), but it is difficult to unpick any one aspect of it because the whole forms a tightly interwoven mass of constraints and assumptions (Fairchild & Kennedy, 2007). In respect of cap carbonates, the narrative is one of rapid deposition in a hothouse Earth in relation to cryosphere meltdown over a period of the order of 10^3 years. An initial kilometre-scale freshwater lid (Yang et al., 2017) overlies seawater rendered saline in the preceding build-up of the cryosphere (Ashkenazy et al., 2013) and takes on the order of 50 000 years to mix with underlying seawater (Yang et al., 2017). The rapid meltdown is a consistent output of modelling studies, yet Hoffman et al. (2017) caution that much less confidence can be placed on models of transients compared with simulations of steady-state conditions. In this paper, sea-floor dolomitisation (requiring a large Mg source) is evidenced at depths shallow enough to be subject to wave action. This is incompatible with such a thick freshwater lid, but would be consistent with a thinner freshwater lid, mixing with underlying seawater by wave action. In the following discussion, it is argued that meltdown on a timescale $>10^4$ years is more consistent with geological data in general and the Svalbard example in particular.

6.2 | Marinoan conditions

A Snowball Earth with ice cover of the order of 1 km thick over the oceans emerges as a stable state in a wide variety of models, whereas 'Waterbelt' solutions with significant open sea water at the equator form under a more restricted range of model configurations (Hoffman et al., 2017). This is a particular challenge in relation to the geological record for the prolonged Sturtian glaciation where abundant examples of open marine deposits in rift basins are found, whereas the shorter Marinoan is dominated by post-rift continental glacial and arid zone deposits (Spence et al., 2016). However, Prave et al. (2016) dated a marine volcanic ash unassociated with glacial sediment in the Marinoan Ghaub Formation deposited 4 Myr before the termination of glaciation. The simplest explanation, preferred by these authors, is that the local marine environment was ice-free.

A way of accommodating geological and modelling results more broadly emerges from the observation that Marinoan glacial successions typically have an unconformity at the base (Spence et al., 2016). Given their low absolute sediment accumulation rates (Partin & Sadler, 2016), this time gap can logically represent most of the duration of the panglaciation corresponding to the most extreme conditions with virtual shutdown of the hydrological cycle (Benn et al., 2015). Hence, the observed sedimentary record may only reflect conditions close to the end of panglaciation (Spence et al., 2016). By use of an intermediate complexity General Circulation Model, Paradise et al. (2019) found that locally temperate conditions could be widespread in Earth-like planets near the snowball exit threshold. In the Svalbard case, ^{17}O-evidence points to the preserved record of glacial advance-retreat cycles in a terrestrial setting being deposited during high PCO_2 conditions over a few precessional cycles (Benn et al., 2015). This complexity is matched by recent data from several independent research groups working on the Yangtze Platform in South China where two or three glacial advance-retreat cycles of Marinoan sediments are documented in both marine and lacustrine contexts with open water conditions during retreat (Chen et al., 2022; Hu et al., 2020; Lang et al., 2018). Ma et al. (2022) explored carbon and pyrite sulphur isotope systematics in depositional units lacking glacial sediment and found patterns of change consistent with waxing and waning of marine productivity. Laminated carbonate beds were reported but not described in these papers, but Gu et al. (2019) reported on the geochemistry of a 1.5 m dolostone bed in the Nantuo Formation of Guizhou province, southern China. It is Mn-rich and overall shows characteristics of suboxic to iron-enriched and anoxic waters. Although likely to be a concretionary bed, this shows the continued capability of the Marinoan ocean to form dolomite.

A consequence of an atmosphere high PCO_2 in contact with unfrozen sediments is an enhancement of chemical weathering processes. Whereas carbonate weathering has a neutral impact on atmospheric PCO_2 because the reaction is reversed during carbonate precipitation, silicate weathering ultimately leads to the removal of excess CO_2 built up from volcanism during panglaciation. A global biogeochemical box model (PreCOSCIOUS, Penman & Rooney, 2019) demonstrated an exponential decline of weathering solute yields over time and emphasises the delivery of aqueous silica (consistent with chert in some cap successions) as well as alkalinity and cations. In a further development of this model, Hood et al. (2021) separately examined Mg and Ca fluxes and found that (marine or terrestrial) silicate weathering was essential to maintain Mg/Ca ratios high enough for the precipitation of dolomite during panglaciation as observed in Sturtian successions. Marine dolomite has also been documented in the Marinoan (Lang et al., 2018) and the consistently dolomitic nature of the Sturtian cap carbonate argues for the same requirements in that panglaciation too. The solutes from silicate weathering fuel reverse weathering reactions acting as a feedback and greatly extending the time of CO_2 drawdown. Direct evidence of enhanced weathering within glacigenic successions is provided by data on bulk composition through

the Chemical Index of Alteration (Bai et al., 2020; Wang et al., 2020). A more specific proxy for intense chemical weathering of silicates is the δ^{26}Mg values with preferential retention of ^{26}Mg in weathering residues. Huang et al. (2016) demonstrated very high δ^{26}Mg values near the top of the Marinoan Nantuo Formation and argued that 97%–99% of atmospheric CO_2 could have been removed by chemical weathering reactions before cap carbonate formation. Li et al. (2020) found lower Mg isotope ratios in the overlying cap carbonate inversely varying with Mg/Al ratios and argued for authigenic silicate formation. Evidence for such reverse weathering reactions have been found lower in the Nantuo Formation, in the drill core studied by Lang et al. (2018); evinced by inverse variation of Li and Mg isotopes (Li et al., 2021). In summary, these new data imply that prior to the sea-level rise that accompanied cap carbonate formation there had already been significant chemical weathering activity and drawdown of atmospheric carbon dioxide, providing a modified boundary condition to be tested in future modelling.

In the Svalbard case, the hyperarid conditions of the Wilsonbreen Formation (Benn et al., 2015; Fairchild et al., 2016b) would have inhibited chemical weathering and there is a negligible clay fraction in siliciclastic rocks. The Wilsonbreen Formation appears to be truncated by surf-zone erosion so that any episode of more intense chemical weathering as inferred by Huang et al. (2016) is unlikely to be preserved both on account of climate and accommodation space. More generally, the Svalbard area offers support for a slower meltdown than inferred in the Snowball model. As expressed by Spence et al. (2016), relatively rapid deglaciation is dependent on three factors: the low latitudes of glaciation, high atmospheric temperatures, and rapid loss of continental ice which had been buttressed at the coast by marine ice. However, a modified perspective stems from the Svalbard fieldwork and modelling in Benn et al. (2015), who demonstrated the influence of precessional forcing and depicted continents where a significant proportion of glacier termini lie inland, rather than at the coast. Hence, one can envisage that the later stages of deglaciation would involve wasting away of ice sheets in continental interiors. Here, the ice sheets may have continued to display precession-related fluctuations and reduced much more rapidly in mass than in surface area. Such a cryosphere, in which sediment would have been trapped in continental interiors, is consistent with a sediment-starved marine cap succession (Nordsvan et al., 2019). In this way, even allowing eustatic sea-level rise to coincide with cap dolostone deposition, the final deglaciation and cap carbonate deposition can be phased over a 10^5 to 10^6 year time frame rather than $<10^4$ years.

6.3 | The meaning of the post-glacial ^{17}O anomaly

The immediate post-Marinoan interval is recognised to be one where glacial meltwater is a significant component in the marine realm (Shields, 2005). The $\Delta^{17}O_{CAS}$ signal in D1 was argued above to be a signature of input of a freshwater end-member to the marine realm, later incorporated in carbonates.

However, evidence for anomalous ^{17}O depletion in early Ediacaran times has come principally from barite which is found in seven of 48 early Ediacaran records (Crockford et al., 2018). These are distributed as seafloor precipitates within a distinct bed, often at the junction between cap dolostone below and limestone above. In south China, the barite-bearing bed rests on a thin cap dolostone bearing a karstic unconformity, and is associated with fibrous dolomite, tepees and sheet cracks (Zhou et al., 2010). Peng et al. (2011) presented a large data set illustrating a range of δ^{34}S and Δ^{17}O values which they interpreted as recording mixing of sulphate carried in by river and barium brought up by upwelling deep water. Subsequent fractionation by microbial sulphate reduction increased the $\delta^{34}S_{CAS}$, and re-oxidation of sulphide reset the Δ^{17}O anomaly. The mixing scenario for the localisation of barite was later confirmed by Ba isotope systematics (Crockford et al., 2019b). A reference section at Wushanhu, southern China, presented by Killingsworth et al. (2013), displays a 1.2 m bed containing barite in which carbon isotope values cross-over from negative to positive. These authors compared with radiometrically dated locations elsewhere in South China, showing the same carbon isotope pattern, to infer that barite deposition happened in a time interval of $2.1 \pm 7.8 \times 10^5$ years.

New data and modelling by Crockford et al. (2016, 2018) demonstrated temporal variation towards a diminishing $\Delta^{17}O_{CAS}$ anomaly and higher δ^{34}S values. These authors modelled the Δ^{17}O variation in terms of a combination of bacterial sulphate reduction leading (trend 1 in Figure 11 to which fit data from Brazil, Norway, Mauritania, North-West Canada and North Australia) and, in the case of Chinese samples, dilution by continent-derived sulphate lacking a significant Δ^{17}O anomaly (3 in Figure 11). This was backed up by ^{33}S-^{34}S systematics which supported the lack of sulphide reoxidation in the model. Much of the small oceanic sulphate reservoir would have been deposited as pyrite in order to explain the strong shift in δ^{34}S from +27‰ to +46‰. The inference that the Δ^{17}O transient could be treated as a globally correlatable event was developed by Crockford et al. (2018).

Interpretation of isotope anomalies in CAS present some additional issues for consideration. One simplifying factor is that, whereas in barite some S could be sourced

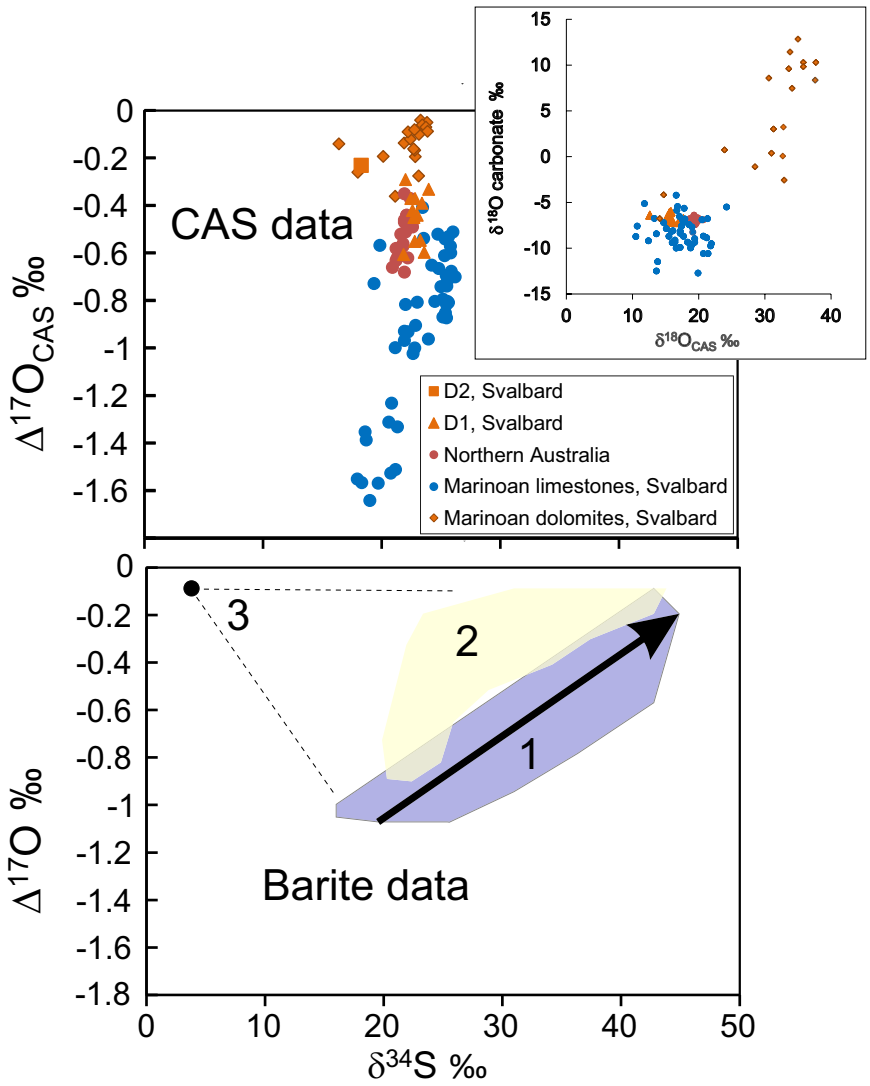

FIGURE 11 $\Delta^{17}O$ and $\delta^{34}S$ data on Marinoan and post-Marinoan sulphate with inset crossplot of $\delta^{18}O$ data from carbonates and CAS; see text for discussion. CAS data shown in top diagram from Benn et al. (2015) [Marinoan data from Svalbard], Bao et al. (2012) [Australia] and herein. The CAS data show a different pattern from the post-Marinoan barite data shown in the lower diagram summarised from Crockford et al. (2016, 2018). Field 1 represents data from Mauritania, North-West Canada, Norway and Brazil with data trends shown by the arrow and attributed to evolution of the global near-surface water body by Crockford et al. (2018). Field 2 represents data from South China which Crockford et al. (2016) attributed to mixing between trend 1 and a hypothetical post-glacial source 3.

from sulphides in upwelling Ba-rich water, the two examples of cap dolostones with negative $\Delta^{17}O$ (Bao et al., 2012 and herein) lack evidence of upwelling. On the other hand, complex mixtures of components with different CAS concentrations and isotope compositions, originating at different stages in diagenesis, can occur in carbonate rocks in general as demonstrated by micro-analysis (Johnson et al., 2021; Rose et al., 2019). However, the two CAS records of cap dolostones are virtually free of pyrite. They present simple patterns (Figure 10), with the only stratigraphic change being an upward decrease in ^{17}O anomaly. The lack of change in $\delta^{34}S$ or $\delta^{18}O$ values points to a lack of diagenetic alteration of the CAS signature, although the concentration of CAS could have been higher in the original $CaCO_3$.

The data of Bao et al. (2012), with the ^{17}O anomaly, derive from the well-known Moonlight Valley unit (Corkeron, 2007; Kennedy, 1996; Williams, 1979) in the Texas/Mabel Downs (TMD) sections in the eastern part of the Kimberley region of Australia, but the anomaly is absent in a section 150 km to the south. The TMD dolostone (8 m thick) appear to be microbially bound and lacks evidence for erosion by wave action. The localised preservation is consistent with the interpretation of Peng et al. (2011) that the anomaly in barite is manifested in locations that are adjacent to continental sources of sulphate.

The CAS data plotted in Figure 11 compare the cap carbonate data with the data from Marinoan (Wilsonbreen Formation) lacustrine and pedogenic dolostones and limestones from Svalbard (Bao et al., 2009; Benn et al., 2015). The Marinoan limestone data were interpreted as reflecting mixtures between pre-existing sulphate on the land surface, lacking a ^{17}O anomaly and sulphate created by oxidation of pyrite and deriving a negative $\Delta^{17}O$ value from atmospheric oxygen. Dolostones in the same context lack the ^{17}O anomaly, but this is clearly a secondary feature because their $\delta^{18}O$ compositions are mostly anomalously high and correlate with the extremely high $\delta^{18}O$ of the carbonate representing an evaporative signal

(Fairchild et al., 2016b). Hence the Wilsonbreen dolostones derived their oxygen mainly from water molecules during re-oxidation following reduction in the environment during the period within which the water was evaporated. The Dracoisen dolostone data, however, compare well with the primary signals from the limestone data in the Wilsonbreen Formation. It follows that the simplest explanation for the post-Marinoan CAS data is that it is a relic feature caused by delayed flushing of the continental sulphate into the marine environment, although a coeval source of sulphate cannot be ruled out. In glacial environments, it is normal to observe 'delayed flow' or 'slowflow' waters seeping from glacial sediment and hydrologically inaccessible portions of glaciers. Where pyrite is present, these waters are highly enriched in sulphate (Fairchild et al., 1999). In the Wilsonbreen environment, a complex topography is inferred and the hyperarid environment, like its modern analogue, the Dry Valleys of Antarctica is expected to display internal drainage (Fairchild et al., 2016b). These are ideal conditions for the delayed flushing of the sulphate $\Delta^{17}O$ signal. A similar interpretation could apply to the Australian data.

It is clear that the traditional correlation of the early Ediacaran succession by carbon isotope signatures is inadequate. Although internally consistent in Svalbard, these are highly variable elsewhere even within a basin (Lang et al., 2016). The proposition of Crockford et al. (2018) that the dying out of the $\Delta^{17}O$ signal offers the best means of correlation in early Ediacaran times is probably valid, albeit complicated by the different patterns of CAS to barite data and the recognition that the signal may be absent in sites remote from freshwater input.

6.4 | Origin of the cap dolostone in Svalbard

For much of the last 25 years there has been a dichotomy of views: either cap carbonate deposition occurred on the 10^3–10^4 timescale reflective of rapid meltdown, or it formed in a sediment-starved context over $>10^5$ years (Fairchild & Kennedy, 2007). There has also been ambiguity in definition of the cap, e.g. where limestone succeeds dolostone in the succession. Part of the case for rapid deposition is the presence in some cap dolostones of a karstic erosion surface and associated clastic sediments interpreted to reflect local isostatic rebound (Shields et al., 2007; Zhou et al., 2010). On the other hand, a complex of clastic sediments partly interfingering with basal cap carbonate in central Australia has been interpreted as the product of many Milankovitch cycles (Kennedy & Christie-Blick, 2011). Either of these interpretations might turn out to be false if, for example, local tectonic factors influenced sedimentation. The unusual continental succession and cap carbonate in south Australia has also caused confusion. A claim of exceptionally fast post-glacial sedimentation was made by Myrow et al. (2018) from South Australia, but this section is actually syn-glacial (Williams & Gostin, 2019) and the sedimentation rates are arguable. A strong argument for slow deposition is posed by repeated magnetic reversals within the cap dolostone, first demonstrated by Trindade et al. (2003). Yu et al. (2020) compared four studies of palaeomagnetic reversals of which the most difficult to explain is that of Terconi, Brazil (Font et al., 2010). Here, an episode of normal polarity interrupts reversed polarity between 11 and 15 m in the 23 m thick cap dolostone whereas the opposite is seen between 6 and 8 m of the 10 m section at Jebel Akhdarin Oman (Kilner et al., 2005). In no case do these data constrain the depositional rate in the lower part of the cap dolostone.

Cutting through this debate is the recent explicit recognition that processes related to high PCO_2 would decline exponentially (Penman & Rooney, 2019) so that substantial changes in rate of formation during cap deposition accommodate much of the disparate evidence presented above. This insight is used to underpin a plausible semi-quantitative sedimentation model for the Svalbard cap (Figure 12). The alkalinity for carbonate production likely derives from many sources (Shields, 2005) of which that from silicate weathering is inadequate to account for the volume of cap carbonate (Le Hir et al., 2009). A combination of carbonate weathering, reversed by planktic and benthic photosynthetic activity in the ocean, coupled with consumption of existing long-term marine alkalinity from iron-reduction (Higgins et al., 2009) and sea-floor weathering and localised methanogenesis seems likely. In the model an exponential decline in carbonate sedimentation is tuned by two constraints. An overall time frame is set by the Re-Os date of 631.2 ± 3.8 Ma on the black shale of Member D3, 104 m above the base of the cap carbonate in Nordaustlandet, that is 3.8 ± 3.8 Myr younger than the 635 Ma age of deglaciation. Carbonate accumulation is tuned to drop exponentially to negligible values at the D2–D3 boundary, identified as the maximum flooding surface by Halverson et al. (2004), around 60 m lower than this stratigraphic height. A second constraint is provided by the 0.95 m thickness of inferred 18 kyr precessional cycles at the D1-D2 boundary (point C on Figure 12) at 22 m height in the Ditlovtoppen section. This is the level at which siliciclastic sediment starts to accumulate, presumably because the water depth is sufficient or sufficient time has passed to permit along-basin circulation of fines from distal fluvial input. In the model, this is depicted as

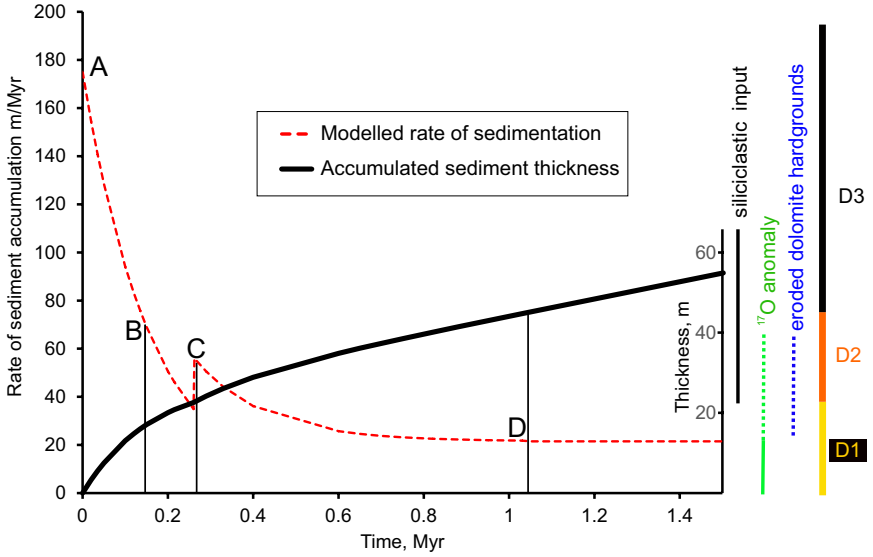

FIGURE 12 Semi-quantitative sediment accumulation model. Assumes exponential decline of carbonate sediment production tracking excess CO_2. (A) Start of cap carbonate accumulation following an initial period of CO_2^-drawdown. (B) First eroded dolostone hardground. (C) Addition of siliciclastic sediment at D1/D2 boundary; at this level inferred 18 kyr precessional cycles are 0.95 m thick. (D) Transition to pure siliciclastic sediment at D2/D3 boundary. Time axis scaled to 104 m sediment accumulation in 3.8 ± 3.8 Myr (Millikin et al., 2022).

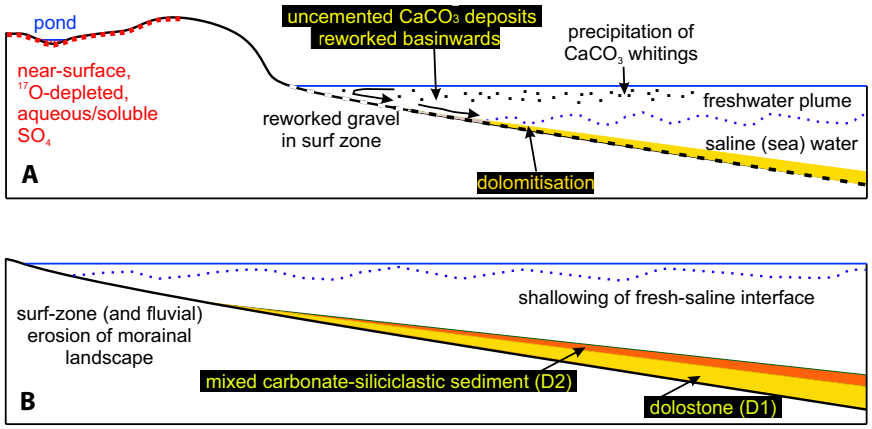

FIGURE 13 Cartoon representations of D1 and D2 environments (not to scale) during post-glacial transgression. (A) Mid-D1 times. Post-glacial sedimentation commences on truncated glacial landscape. Glacial meltwater creates freshwater plume on seawater, but nearby terrestrial areas with internal drainage retain ^{17}O-depleted sulphate in water bodies and near-surface environments. Calcium carbonate whitings settle towards the sea bed but are readily reworked by waves and storms leading to overall offshore transport. In more stable offshore environments, dolomitisation close to sediment surface occurs in seawater-dominated fluid and is exposed by storm erosion. (B) D2 times. More extensive erosion of morainic glacial landscape but meltwater production, sea-level rise and carbonate production are all reduced. A distal fluvial source of fine sediment mixes with a reduced flux of carbonate sediments. $CaCO_3$ precipitation and dolomite formation continue (not explicitly shown).

a step change in accumulation with the siliciclastic input at a fixed rate of ≈2 cm/kyr. These values allow the exponential decline of carbonate accumulation to merge imperceptibly into background siliciclastic sedimentation at the D2-D3 boundary at position D in Figure 12, just over a million years after the onset of sea-level rise. The model depicts a dramatic fall in sediment accumulation rates. The initial rate approaches 200 m/My (20 cm/kyr), but falls by a factor of three by Point B (Figure 12) after *ca* 150 000 years, that is by the time the first dolostone hardgrounds are present and where the ^{17}O anomaly (Figure 10C) is largely attenuated. This time presumably coincides with a condition whereby only a small proportion of freshwater is mixed in seawater at the sea bed.

A cartoon model of processes responsible for the cap environments is shown in Figure 13. Here are depicted

two snapshots of the marine transgression across the preserved basin margin. Because of the lack of preservation of deep portions of the basin, the cap dolostone accumulation (Figure 13A) represents a period after the fastest initial transgression. The Svalbard-North-East Greenland basin is characterised by its simple facies patterns along the margins of what may have been a relatively narrow basin. The lack of barite in the succession, or other indicators of deep marine hydrothermal activity such as Mn-enrichments (Ning et al., 2021) implies a lack of access to strongly upwelling deep water. The simple pattern of slightly decreasing $\delta^{13}C$ with time, could simply reflect an overall depth effect (Lang et al., 2016).

At this stage an untransgressed glacial hinterland bearing sulphate with negative $\Delta^{17}O$ values was still present. Calcium carbonate was precipitated readily in whitings in the fresh surface waters (Shields, 2005) but there was only net accumulation offshore because of wave and storm action. Sediment that was undisturbed for long enough was bound microbially and once a water sufficiently rich in Mg was encountered, dolomitisation proceeded. Intermittent storm action exposed dolostone hardgrounds and created peloidal sediment. In D2 times (Figure 13B), the transgression led to submergence of the nearby continent and the termination of input of sulphate with negative $\Delta^{17}O$ signature. By now, fine siliciclastic sediment had entered the basin and carbonate sediment tailed off in the offshore setting. The cap carbonate departed with a whimper.

7 | CONCLUSIONS

The cap carbonate to Marinoan glacial deposits in North-East Svalbard is dominated by parallel-laminated dolostones representing the deposits of energetic storm-generated flows, partly stabilised by microbial binding. Pauses in sedimentation promoted lithification by dolomicrospar, locally exposed as hardground surfaces. The dolomite chemistry reflects that of the depositional water, modified by early diagenetic redox reactions in pore waters. A fall in $\delta^{13}C$ values from −3 to −5‰ reflects some combination of time-evolution and deeper water conditions. Carbonate-associated sulphate displays a time-varying negative $\Delta^{17}O$ anomaly, only the second to be described in cap carbonates. It is interpreted to have been generated in contact with the atmosphere in a continental environment and has comparable isotope characteristics to the anomaly in underlying Marinoan carbonates deposited in glacial settings. The CAS signal thus provides evidence for a freshwater signal in post-glacial marine environments, but the dolomite mineralogy of the cap implies a dominance of a saline Mg-rich component in shallow seas. A semi-quantitatively calibrated model of exponentially declining carbonate production allows the cap to be reconciled with opposing theoretical visions of the rate of sedimentation: initial deposition was rapid (approaching 20 cm/kyr), dropped by a factor of 3 by the time the freshwater input had minimised, and ultimately faded out on the million-year timescale.

ACKNOWLEDGEMENTS

Fieldwork in 2010–2011 was supported by the UK's Natural Environment Research Council-funded project GR3/NE/H004963/1 Glacial Activity in Neoproterozoic Svalbard (GAINS). Emily McMillan, Peter Wynn, and Yongbo Peng are thanked for assistance in laboratory analyses. Referees Adrian Immenhauser and Malcolm Wallace are thanked for their encouragement and positive suggestions for improvement of the manuscript. As this is a special issue in honour of Tony Dickson, IJF is proud to record that he was Tony's first research student and was thereby transfused with life-long enthusiasm for carbonate fieldwork, petrology and geochemistry.

DATA AVAILABILITY STATEMENT

Data sharing is not applicable to this article as no new data were created or analyzed in this study.

ORCID

Ian J. Fairchild https://orcid.org/0000-0003-4822-2895

REFERENCES

Algeo, T.J. & Liu, J. (2020) A re-assessment of elemental proxies for paleoredox analysis. *Chemical Geology*, *540*, 119549. https://doi.org/10.1016/j.chemgeo.2020.119549

Allen, P.A. & Hoffman, P.F. (2005) Extreme winds and waves in the aftermath of a Neoproterozoic glaciation. *Nature*, *433*, 123–127.

Ahm, A.-S.C., Bjerrum, C.J., Blättler, C.L., Swart, P.K. & Higgins, J.A. (2018) Quantifying early marine diagenesis in shallow-water carbonate sediments. *Geochimica et Cosmochimica Acta*, *236*, 140–159.

Ahm, A.-S.C., Maloof, A.C., Macdonald, F.A., Hoffman, P.F., Bjerrum, C.J., Bold, U., Rose, C.V., Strauss, J.V. & Higgins, J.A. (2019) An early diagenetic deglacial origin for basal Ediacaran "cap dolostones". *Earth and Planetary Science Letters*, *506*, 292–307.

Ashkenazy, Y., Gildor, H., Losch, M., Macdonald, F.A., Schrag, D.P. & Tziperman, E. (2013) Dynamics of a snowball earth ocean. *Nature*, *495*, 90–93. https://doi.org/10.1038/nature11894

Bai, H., Kuang, H., Liu, Y., Peng, N., Chen, X. & Wang, Y. (2020) Marinoan-aged red beds at Shennongjia, South China: evidence against global-scale glaciation during the Cryogenian. *Palaeogeography, Palaeoclimatology, Palaeoecology*, *559*, 109967. https://doi.org/10.1016/j.palaeo.2020.109967

Bao, H., Lyons, J.R. & Zhou, C. (2008) Triple oxygen isotope evidence for elevated CO_2 levels after a Neoproterozoic glaciation. *Nature*, *453*, 504–506.

Bao, H., Fairchild, I.J., Wynn, P.M. & Spötl, C. (2009) Stretching the envelope of past surface environments: Neoproterozoic glacial lakes from Svalbard. *Science*, *323*, 119–122.

Bao, H., Chen, Z.Q. & Zhou, C. (2012) An ^{17}O record of late Neoproterozoic glaciation in the Kimberley region, Western Australia. *Precambrian Research*, *216–219*, 152–161.

Barnaby, R.J. & Rimstidt, J.D. (1989) Redox conditions of calcite cementation interpreted from Mn and Fe contents of authigenic calcites. *Geological Society of America Bulletin*, *101*, 795–804.

Benn, D.I., Le Hir, G., Bao, H., Donnadieu, Y., Dumas, C., Fleming, E.J., Hambrey, M.J., McMillan, E.A., Petronis, M.S., Ramstein, G., Stevenson, C.T.E., Wynn, P.M. & Fairchild, I.J. (2015) Orbitally forced Ice sheet fluctuations at the end of the Marinoan Snowball Earth glaciation. *Nature Geoscience*, *8*, 704–707.

Budyko, M.I. (1969) The effect of solar radiation variations on the climate of the Earth. *Tellus*, *21*, 611–619.

Burdige, D.J. (1993) The biogeochemistry of manganese and iron reduction in marine sediments. *Earth-Science Reviews*, *35*, 249–284.

Canfield, D.E., Poulton, S.W. & Narbonne, G.M. (2007) Late-Neoproterozoic deep-ocean oxygenation and the rise of animal life. *Science*, *315*, 92–95.

Cao, X. & Bao, H. (2013) Dynamic model constraints on ^{17}O depletion in atmospheric O_2 after a snowball Earth. *Proceedings of the National Academy of Sciences of the USA*, *110*, 14546–14550.

Chen, X., Zhou, Y. & Shields, G.A. (2022) Progress towards an improved Precambrian seawater $^{87}Sr/^{86}Sr$ curve. *Earth-Science Reviews*, *2022*, 103869. https://doi.org/10.1016/j.earscirev.2021.103869

Corkeron, M. (2007) 'Cap carbonates' and Neoproterozoic glacigenic successions from the Kimberley region, north-west Australia. *Sedimentology*, *54*, 871–903.

Crockford, P.W., Cowie, B.R., Johnston, D.T., Hoffman, P.F., Sugiyama, I., Pellerin, A., Bui, T.H., Hayles, J., Havlerson, G.P., Macdonald, F.A. & Wing, B.A. (2016) Triple oxygen and multiple sulfur isotope constraints on the evolution of the post-Marinoan sulfur cycle. *Earth and Planetary Science Letters*, *435*, 74–83.

Crockford, P.W., Hodgkiss, M.S.W., Uhlein, G.J., Caxito, F., Hayles, J.A. & Halverson, G.P. (2018) Linking paleocontinents through triple oxygen isotope anomalies. *Geology*, *46*, 179–182.

Crockford, P.W., Kunzmann, M., Bekker, A., Hayles, J., Bao, H., Halverson, G.P., Peng, Y., Bui, T.H., Cox, G.M., Gibson, T.M., Wörndle, S., Rainbird, R., Lepland, A., Swanson-Hysell, N.L., Mater, S., Sreenivas, B., Kuznetsov, A., Krupenik, V. & Wing, B.A. (2019a) Claypool continued: extending the isotopic record of sedimentary sulfate. *Chemical Geology*, *513*, 200–225.

Crockford, P.W., Wing, B.A., Paytan, A., Hodgkiss, M.S.W., Mayfield, K.J., Hayles, J.A., Middleton, J.E., Ahm, A.-S.C., Johnston, D.T., Caxito, F., Uhlein, G., Halverson, G.P., Eickmann, B., Torres, M. & Horner, T.J. (2019b) Barium-isotopic constraints on the origin of post-Marinoan barites. *Earth and Planetary Science Letters*, *519*, 234–244.

Daye, M., Higgins, J. & Bosak, T. (2019) Formation of ordered dolomite in anaerobic photosynthesis biofilms. *Geology*, *47*, 509–512.

Deynoux, M. (1982) Periglacial polygonal structures and sand wedges in the late Precambrian glacial formations of the Taoudeni Basin in Adrar of Mauretania (West Africa). *Palaeogeography, Palaeoclimatology, Palaeoecology*, *39*, 55–70.

Dupraz, C., Reid, R.P., Braissnat, O., Decho, A.W., Norman, R.S. & Visscher, P.T. (2009) Processes of carbonate precipitation in modern microbial mats. *Earth-Science Reviews*, *96*, 141–162.

Edwards, M.B. (1976) Sedimentology of Late Precambrian Sveanor and Kapp Sparre Formations at Aldousbreen, Wahlenbergfjorden, Nordaustlandet. *Norsk Polarinstitutt Årbok*, *1974*, 51–61.

Fairchild, I.J. (1983) Chemical controls of cathodoluminescence of natural dolomites and calcites: new data and review. *Sedimentology*, *30*, 579–583.

Fairchild, I.J. (1993) Balmy shores and icy wastes: the paradox of carbonates associated with glacial deposits in Neoproterozoic times. *Sedimentology Review*, *1*, 1–16.

Fairchild, I.J. & Hambrey, M.J. (1984) The Vendian succession of northeastern Spitsbergen – petrogenesis of a dolomite-tillite association. *Precambrian Research*, *26*, 111–167.

Fairchild, I.J. & Spiro, B. (1987) Petrological and isotopic implications of some contrasting Precambrian carbonates, NE Spitsbergen. *Sedimentology*, *34*, 973–989.

Fairchild, I.J. & Hambrey, M.J. (1995) Vendian basin evolution in East Greenland and NE Svalbard. *Precambrian Research*, *73*, 217–233.

Fairchild, I.J. & Kennedy, M.J. (2007) Neoproterozoic glaciation in the Earth System. *Journal of the Geological Society, London*, *164*, 895–921.

Fairchild, I.J., Killawee, J.A., Sharp, M.J., Spiro, B., Hubbard, B.P., Lorrain, R.D. & Tison, J.-L. (1999) Solute generation and transfer from a chemically reactive Alpine glacial-proglacial system. *Earth Surface Processes and Landforms*, *24*, 1189–1211.

Fairchild, I.J., Bonnand, P., Davies, T., Fleming, E.J., Grassineau, N., Halverson, G.P., Hambrey, M.J., McMillan, E.A., McKay, E., Parkinson, I.J. & Stevenson, C.T.E. (2016a) The Late Cryogenian Warm Interval, NE Svalbard: chemostratigraphy and genesis of dolomitic shales. *Precambrian Research*, *281*, 128–154.

Fairchild, I.J., Fleming, E.J., Bao, H., Benn, D.I., Boomer, I., Dublyansky, Y.V., Halverson, G.P., Hambrey, M.J., Hendy, C., McMillan, E.A., Spötl, C., Stevenson, C.T.E. & Wynn, P.M. (2016b) Continental carbonate facies of a Neoproterozoic panglaciation, NE Svalbard. *Sedimentology*, *63*, 443–497.

Fichtner, V., Strauss, H., Immenhauser, A., Buhl, D., Neuser, R.D. & Niedermayr, A. (2017) Diagenesis of carbonate associated sulfate. *Chemical Geology*, *463*, 61–75.

Fleming, E.J., Benn, D.I., Stevenson, C.T.E., Petronis, M.S., Hambrey, M.J. & Fairchild, I.J. (2016) Glacitectonism, subglacial and glacilacustrine processes during a Neoproterozoic panglaciation, northeast Svalbard. *Sedimentology*, *63*, 411–442.

Font, E., Nédélec, A., Trindade, R.I.F. & Moreau, C. (2010) Fast or slow melting of the Marinoan snowball Earth? The cap dolostone record. *Palaeogeography, Palaeoclimatology, Palaeoecology*, *295*, 215–225.

Gu, S.Y., Fu, Y. & Long, J.X. (2019) Predominantly ferruginous conditions in South China during the Marinoan glaciation: insight from REE geochemistry of the syn-glacial dolostone from the Nantuo Formation in Guizhou Province, China. *Minerals*, *9*, article 348. https://doi.org/10.3390/min9060348

Halverson, G.P. (2011) Glacial sediments and associated strata of the Polarisbreen Group, northeastern Svalbard. In: Arnaud, E., Halverson, G.P. & Shields-Zhou, G. (Eds.) *The geological record*

of neoproterozoic glaciations, *36*. London: Geological Society, pp. 571–579.

Halverson, G.P., Maloof, A.C. & Hoffman, P.F. (2004) The Marinoan glaciation (Neoproterozoic) in northeast Svalbard. *Basin Research*, *16*, 297–324.

Halverson, G.P., Hoffman, P.F., Schrag, D.P. & Maloof, A.C. (2005) Towards a Neoproterozoic composite carbon-isotope record. *Geological Society of America Bulletin*, *117*, 1181–1207. https://doi.org/10.1130/B25630.1

Halverson, G.P., Kunzmann, M., Strauss, J.V. & Maloof, A.C. (2018) The Tonian-Cryogenian transition in Northeastern Svalbard. *Precambrian Research*, *319*, 79–95.

Halverson, G.P., Porter, S. & Shields, G.A. (2020) The Tonian and Cryogenian periods, chapter 17. In: Gradstein, F.M., Ogg, J.G., Schmitz, M. & Ogg, G. (Eds.) *Geological time scale 2020*. Amsterdam: Elsevier, pp. 495–519. https://doi.org/10.1016/B978-0-12-824360-2.00017-6

Hambrey, M.J. & Spencer, A.M. (1987) Late Precambrian glaciation of central East Greenland. *Meddelelser om Grønland*, *19*, 1–50.

Harland, W.B., Scott, R.A., Auckland, K.A. & Snape, I. (1992) The Ny Friesland Orogen, Spitsbergen. *Geological Magazine*, *129*, 679–708.

Harland, W.B., Hambrey, M.J. & Waddams, P. (1993) Vendian geology of Svalbard. *Norsk Polarinstitutt Skrifter*, *193*, 1–150.

He, R., Lang, X. & Shen, B. (2021) A rapid rise of seawater δ^{13}C during the deglaciation of the Marinoan Snowball Earth. *Global and Planetary Change*, *207*, 103672. https://doi.org/10.1016/j.gloplacha.2021.103672

Higgins, J.A., Fischer, W.W. & Schrag, D.P. (2009) Oxygenation of the ocean and sediments: consequences for the seafloor carbonate factory. *Earth and Planetary Science Letters*, *284*, 25–33.

Higgins, J.A., Blättler, C.L., Lundstrom, E.A., Santiago-Ramos, D.P., Akhtar, A.A., Crüger Ahm, A.-S., Bialik, O., Holmden, C., Bradbury, H., Murray, S.T. & Swart, P.K. (2018) Mineralogy, early marine diagenesis, and the chemistry of shallow-water carbonate sediments. *Geochimica et Cosmochimica Acta*, *220*, 512–534.

Hoffman, P.F. & Schrag, D.P. (2002) The snowball Earth hypothesis: testing the limits of global change. *Terra Nova*, *14*, 129–155.

Hoffman, P.F. & Lamothe, K.G. (2019) Seawater-buffered diagenesis, destruction of carbon isotope excursions, and the composition of DIC in Neoproterozoic oceans. *Proceedings of the National Academy of Sciences of the USA*, *116*, 18874–18879. https://doi.org/10.1073/pnas.1909570116

Hoffman, P.F., Kaufman, A.J., Halverson, G.P. and Schrag, D.P. (1998) A Neoproterozoic snowball earth. *Science*, *281*, 1342–1346.

Hoffman, P.F., Halverson, G.P., Domack, E.W., Husson, J.M., Higgins, J.A. & Schrag, D.P. (2007) Are basal Ediacaran (635 Ma) post-glacial "cap dolostones" diachronous? *Earth and Planetary Science Letters*, *258*, 114–131.

Hoffman, P.F., Halverson, G.P., Domack, E.W., Maloof, A.C., Swanson-Hysell, N.L. & Cox, G.M. (2012) Cryogenian glaciations on the southern tropical paleomargin of Laurentia (NE Svalbard and East Greenland), and a primary origin for the upper Russøya (Islay) carbon isotope excursion. *Precambrian Research*, *206-207*, 137–158.

Hoffman, P.F., Abbot, D.S., Ashkenazy, Y., Benn, D.I., Cohen, P.A., Cox, G.M., Creveling, J.R., Donnadieu, Y., Erwin, D.H., Fairchild, I.J., Ferreira, D., Goodman, J.C., Halverson, G.P., Jansen, M.F., Le Hir, G., Love, G.D., Macdonald, F.A., Maloof, A.C., Ramstein, G., Rose, B.E.J., Rose, C.V., Tziperman, E., Voigt, A. & Warren, S.G. (2017) Climate dynamics of Snowball Earth and Cryogenian geology–geobiology. *Science Advances*, *3*, e1600983.

Hoffman, P.F., Halverson, G.P., Scrag, D.P., Higgins, J.A., Domack, E.W., Macdonald, F.A., Pruss, S.B., Blättler, C.L., Crockford, P.W., Hodgin, E.B., Bellefroid, E.J., Johnson, B.W., Hodgkiss, M.S.W., Lamothe, K.G., LoBianco, S.J.C., Busch, J.F., Howes, B.J., Greenman, J.W. & Nelson, L.L. (2021) Snowballs in Africa: sectioning a long-lived Neoproterozoic carbonate platform and its bathyal foreslope. *Earth-Science Reviews*, *218*, 103616.

Hood, A.V.S. & Wallace, M.W. (2015) Extreme ocean anoxia during the Late Cryogenian recorded in reefal carbonates of Southern Australia. *Precambrian Research*, *261*, 96–111.

Hood, A.v.S. & Wallace, M.W. (2018) Neoproterozoic marine carbonates and their paleoceanographic significance. *Global and Planetary Change*, *160*, 28–45.

Hood, A.v.S., Penman, D.E., Lechte, M.A., Wallace, M.W., Giddings, J.A. & Planavsky, N.J. (2021) Neoproterozoic syn-glacial carbonate precipitation and implications for a snowball Earth. *Geobiology*. https://doi.org/10.1111/gbi.12470

Hu, Y., Cai, C., Liu, D., Pederson, C.L., Jiang, L., Shen, A. & Immenhauser, A. (2020) Formation, diagenesis and palaeoenvironmental significance of upper Ediacaran fibrous dolomite cements. *Sedimentology*, *67*, 1161–1187.

Hurtgen, M.T, Arthur, M.A., Suits, N.S., and Kaufman, A.J., (2002) The sulfur isotopic composition of Neoproterozoic seawater sulfate: impl.ications for a snowball Earth. *Arth and Planetary Science Letters*, *203*, 413–429.

Huang, K.-J., Teng, F.-Z., Shen, B., Xiao Land, X., Ma, H.-R., Fu, Y. & Peng, Y. (2016) Episode of intense chemical weathering during the termination of the 635 Ma Marinoan glaciation. *Proceedings of the National Academy of Sciences of the USA*, *113*, 14904–14909.

James, N.P., Narbonne, G.M. & Kyser, T.K. (2001) Late Neoproterozoic cap carbonates: Mackenzie Mountains, northwestern Canada: precipitation and global glacial meltdown. *Canadian Journal of Earth Sciences*, *38*, 1229–1262.

Jin, C., Li, C., Algeo, T.J., O'Connell, B., Cheng, M., Shi, W., Shen, J. & Planavasky, N.J. (2018) Highly heterogeneous "poikiloredox" conditions in the early Ediacaran Yangtze Sea. *Precambrian Research*, *311*, 157–166.

John, S.G., Kunzmann, M., Townsend, E.J. & Rosenberg, A.D. (2017) Zinc and cadmium stable isotopes in the geological record: a case study from the post-snowball Earth Nuccaleena cap dolostone. *Palaeogeography, Palaeoclimatology, Palaeoecology*, *466*, 202–208.

Johnson, D.L., Present, T.M., Li, M., Shen, Y. & Adkins, J.F. (2021) Carbonate associated sulfate (CAS) δ^{34}S heterogeneity across the End-Permian Mass Extinction in South China. *Earth and Planetary Science Letters*, *574*, 117172. https://doi.org/10.1016/j.epsl.2021.117172

Kennedy, M.J. (1996) Stratigraphy, sedimentology, and isotopic geochemistry of Australian Neoproterozoic cap dolostones: deglaciation, δ^{13}C excursions, and carbonate precipitation. *Journal of Sedimentary Research*, *66*, 1050–1064.

Kennedy, M.J. & Christie-Blick, N. (2011) Condensation origin for Neoproterozoic cap carbonates during deglaciation. *Geology*, *39*, 319–322.

Kennedy, M.J., Runnegar, B., Prave, A.R., Hoffman, K.H. & Arthur, M. (1998) Two or four Neoproterozoic glaciations? *Geology*, *26*, 1059–1063.

Killingsworth, B.A., Hayles, J.A., Zhou, C. & Bao, H. (2013) Sedimentary constraints on the duration of the Marinoan ^{17}O depletion (MOSD) event. *Proceedings of the National Academy of Sciences of the USA*, *110*, 17686–17690.

Kilner, B., Niocaill, C. & Brasier, M. (2005) Low-latitude glaciation in the Neoproterozoic of Oman. *Geology*, *33*, 413–416.

Knoll, A.H., Hayes, J.M., Kaufman, A.J., Swett, K. & Lambert, I.B. (1986) Secular variations in carbon isotope ratios from Upper Proterozoic successions of Svalbard and east Greenland. *Nature*, *321*, 832–837.

Knoll, A.H., Walter, M.R., Narbonne, G.M. & Christie-Blick, N. (2006) The Ediacaran Period: a new addition to the geologic time scale. *Lethaia*, *39*, 13–30.

Krause, S., Liebetrau, V., Gorb, S., Sánchez-Román, M.N., McKenzie, J.A. & Treude, T. (2012) Microbial nucleation of Mg-rich dolomite in exopolymeric substances under anoxic modern seawater salinity: new insight into an old enigma. *Geology*, *40*, 587–590.

Kuang, H., Liu, Y., Peng, N., Vandyk, T.M., Le Heron, D.P., Zhu, Z., Bai, H., Wang, Y., Wang, Z., Zhong, Q., Chen, J., Yu, H., Chen, X., Song, C. & Qi, K. (2022) Ediacaran cap dolomite of Shennongjia, northern Yangtze Craton, South China. *Precambrian Research*, *368*, 106483. https://doi.org/10.1016/j.precamres.2021.106483

Kunzmann, M., Halverson, G.P., Scott, C., Minarik, W.G. & Wing, B.A. (2015) Geochemistry of Neoproterozoic black shales from Svalbard: implications for oceanic redox conditions spanning Cryogenian glaciations. *Chemical Geology*, *417*, 383–393.

Kunzmann, M., Gibson, T.M., Halverson, G.P., Hodgkiss, M.S.W., Bui, T.H., Carozza, D.A., Sperling, E.A., Poirier, A., Cox, G.M. & Wing, B.A. (2017a) Iron isotope biogeochemistry of Neoproterozoic marine shales. *Geochimica et Cosmochimica Acta*, *209*, 85–105.

Kunzmann, M., Bui, T.H., Crockford, P.W., Halverson, G.P., Scott, C., Lyons, T.W. & Wing, B.A. (2017b) Bacterial sulfur disproportionation constrains timing of Neoproterozoic oxygenation. *Geology*, *45*, 207–210.

Lamb, M.P., Fischer, W.W., Raub, T.D., Taylor Perron, J. & Myrow, P.M. (2012) Origin of giant wave ripples in snowball Earth cap carbonate. *Geology*, *40*, 827–830. https://doi.org/10.1130/G33093.1

Lang, X., Shen, B., Peng, Y., Huang, K., Lv, J. & Ma, H. (2016) Ocean oxidation during the deposition of basal Ediacaran Doushantuo cap carbonates in the Yangtze Platform, South China. *Precambrian Research*, *281*, 253–268.

Lang, X., Chen, J., Cui, H., Man, L., Huang, K.-J., Fu, Y., Zhou, C. & Shen, B. (2018) Cyclic cold climate during the Nantuo Glaciation: evidence from the Cryogenian Nantuo Formation in the Yangtze Block, South China. *Precambrian Research*, *310*, 243–255.

Le Hir, G., Donnadieu, Y., Goddéris, Y., Pierrehumbert, R.T., Halverson, G.P., Macouin, M., Nédélec, A. & Ramstein, G. (2009) The Snowball Earth aftermath: exploring the limits of continental weathering processes. *Earth and Planetary Science Letters*, *277*, 453–463.

Li, F., Penman, D., Planavsky, N., Knudsen, A., Zho, M., Wang, X., Isson, T., Huang, K., Wei, G., Zhang, S., Shen, J., Zhu, X. & Shen, B. (2021) Reverse weathering may amplify post-Snowball atmospheric carbon dioxide levels. *Precambrian Research*, *364*, 106279.

Li, J., Hao, C., Wang, Z., Dong, L., Wang, Y., Huang, K.-J., Lang, X., Huang, T., Yuan, H., Zhou, C. & Shen, B. (2020) Continental weathering intensity during the termination of the Marinoan Snowball Earth: Mg isotope evidence from the basal Doushantuo cap carbonate in South China. *Palaeogeography, Palaeoclimatology, Palaeoecology*, *552*, 109774. https://doi.org/10.1016/j.palaeo.2020.109774

Ma, H., Shen, B., Lang, X., Peng, Y., Huang, K., Huang, T., Fu, Y. & Tang, W. (2022) Active biogeochemical cycles during the Marinoan global glaciation. *Geochimica et Cosmochimica Acta*, *321*, 155–169.

Mackey, T.J., Jost, A.B., Creveling, J.R. & Bergmann, K.D. (2020) A decrease to low carbonate clumped isotope temperatures in Cryogenian strata. *AGU Advances*, *1*, e2019AV000159. https://doi.org/10.1029/2019AV000159

Millikin, A.E.G., Strauss, J.V., Halverson, G.P., Bergmann, K.D., Tosca, N.J. & Rooney, A.D. (2022) Calibrating the Russøya excursion in Svalbard, Norway and implications for Neoproterozoic chronology. *Geology*, *50*, 506–510. https://doi.org/10.1130/G49593.1

Murray, S.T., Higgins, J.A., Holmden, C., Lu, C. & Swart, P.K. (2021) Geochemical fingerprints of dolomitization in Bahamian carbonates: evidence from sulphur, calcium, magnesium and clumped isotopes. *Sedimentology*, *68*, 1–29.

Myrow, P.M., Lamb, M.P. & Ewing, R.C. (2018) Rapid sea level rise in the aftermath of a Neoproterozoic snowball Earth. *Science*, *360*, 649–651.

Ning, M., Yang, F., Ma, H., Land, X. & Shen, B. (2021) Precipitation of Marinoan cap carbonate from Mn-enriched seawater. *Earth-Science Reviews*, *218*, 103666. https://doi.org/10.1016/j.earscirev.2021.103666

Nordsvan, A.R., Barham, M., Cox, G., Kirscher, U. & Mitchell, R.N. (2019) Major shoreline retreat and sediment starvation following Snowball Earth. *Terra Nova*, *31*, 495–502. https://doi.org/10.1111/ter.12426

Paradise, A., Menou, K., Valencia, D. & Lee, C. (2019) Habitable snowballs: temperate land conditions, liquid water and implications for CO_2 weathering. *Journal of Geophysical Research: Planets*, *124*, 2087–2100. https://doi.org/10.1029/2019JE005917

Partin, C.A. & Sadler, P.M. (2016) Slow net sediment accumulation sets snowball Earth apart from younger glacial episodes. *Geology*, *44*, 1019–1022.

Peng, Y., Bao, H., Zhou, C. & Yuan, X. (2011) ^{17}O-depleted barite from two Marinoan cap dolostone sections, South China. *Earth and Planetary Science Letters*, *305*, 21–31.

Penman, D.R. & Rooney, A.D. (2019) Coupled carbon and silica cycle perturbations during the Marinoan snowball Earth deglaciation. *Geology*, *47*, 317–320.

Petrash, D.A., Bialik, O.M., Bontognaili, T.R.R., Vasconcelos, C., Roberts, J.A., McKenzie, J.A. & Konhauser, K. (2017) Microbially catalyzed dolomite formation: from near-surface to burial. *Earth-Science Reviews*, *171*, 558–582.

Prave, A.R., Condon, D.J., Hoffmann, K.H., Tapster, S. & Fallick, A.E. (2016) Duration and nature of the end-Cryogenian (Marinoan) glaciation. *Geology*, *44*, 631–634.

Richter, D.K., Götte, T., Götze, J. & Neuser, R.D. (2003) Progress in application of cathodoluminescence in sedimentary petrology. *Mineralogy and Petrology*, *79*, 127–166.

Rose, C.V. & Maloof, A.C. (2010) Testing models for post-glacial 'cap dolostone' deposition: Nuccaleena Formation, South Australia. *Earth and Planetary Science Letters*, *296*, 165–180.

Rose, C.V., Webb, S.M., Newville, M., Lanzirotti, A., Richardson, J.A., Tosca, N.J., Catalona, J.G., Bradley, A.S. & Fike, D.A. (2019) Insights into past ocean proxies from micron-scale mapping of sulfur species in carbonates. *Geology*, *47*, 833–837. https://doi.org/10.1130/G46228.1

Sahoo, S.K., Planavsky, N.J., Kendall, B., Wang, X., Shi, X., Scott, C.T., Anbar, A.D., Lyons, T.W. & Jiang, G. (2012) Ocean oxygenation in the wake of the Marinoan glaciation. *Nature*, *489*, 546–549.

Shields, G.A. (2005) Neoproterozoic cap carbonates: a critical appraisal of existing models and the plumeworld hypothesis. *Terra Nova*, *17*, 299–310.

Shields, G.A., Deynoux, M., Strauss, H., Paquet, H. & Nahon, D. (2007) Barite-bearing dolostones of the Taoudéni Basin, northwest Africa: sedimentary and isotopic evidence for methane seepage after a Neoproterozoic glaciation. *Precambrian Research*, *153*, 209–235.

Shuster, A.M., Wallace, M.W., van Smeerdijk Hood, A. & Jiang, G. (2018) The Tonian Beck Spring Dolomite: marine dolomitization in a shallow, anoxic sea. *Sedimentary Geology*, *368*, 83–104.

Spence, G.H., Le Heron, D.P. & Fairchild, I.J. (2016) Sedimentological perspectives on climatic, atmospheric and environmental change in the Neoproterozoic era. *Sedimentology*, *63*, 253–306.

Swanner, E.D., Lambrecht, N., Wittkop, C., Harding, C., Katsev, S., Torgeson, J. & Poulton, S.W. (2020) The biogeochemistry of ferruginous lakes and past ferruginous oceans. *Earth-Science Reviews*, *211*, 103430. https://doi.org/10.1016/j.earscirev.2020.103430

Tahata, M., Sawaki, Y., Yoshiya, K., Nishizawa, M., Komiya, T., Hirata, T., Yoshida, N., Maruyama, S. & Windley, B.F. (2015) The marine environments encompassing the Neoproterozoic glaciations: evidence from C, Sr and Fe isotope ratios in the Hecla Hoek Supergroup in Svalbard. *Precambrian Research*, *263*, 19–42.

Thiemens, M. (1983) The mass-independent fractionation of oxygen: a novel isotope effect and its possible cosmochemical implications. *Science*, *219*, 1073–1075.

Trindade, R.I.F., Font, E., D'Agrella, M.S., Nogueira, A.C.R. & Riccomini, C. (2003) Low-latitude and multiple geomagnetic reversals in the Neoproterozoic Puga cap carbonate, Amazon craton. *Terra Nova*, *15*, 441–446.

Tucker, M.E. (1982) Precambrian dolomites: petrographic and isotopic evidence that they differ from Phanerozoic dolomites. *Geology*, *10*, 7–12.

Voigt, A. & Abbot, D.S. (2012) Sea-ice dynamics strongly promote Snowball Earth initiation and destabilize tropical sea-ice margins. *Climates of the Past*, *8*, 2079–2092.

Wallmann, K., Aloisi, G., Haeckel, M., Tishchenko, P., Pavlova, G., Greinert, J., Kutterolf, S. & Eisenhauer, A. (2008) Silicate weathering in anoxic marine sediments. *Geochimica et Cosmochimica Acta*, *72*, 2895–2918.

Wallace, M.W., Hood, A.V.S., Shuster, A., Greig, A., Planavsky, N.J. & Reed, C.P. (2017) Oxygenation history of the Neoproterozoic to early Phanerozoic and the rise of land plants. *Earth and Planetary Science Letters*, *466*, 12–19.

Wallace, M.W., Hood, A.V.S., Fayle, J., Horden, E.S. & O'Hare, T.F. (2019) Neoproterozoic marine dolomite hardgrounds and their relationship to cap dolomites. *Precambrian Research*, *328*, 269–286.

Waltham, D. (2015) Milankovitch period uncertainties and their impact on cyclostratigraphy. *Journal of Sedimentary Research*, *85*, 990–998.

Wang, P., Du, Y., Yu, W., Algeo, T.J., Zhou, Q., Xu, Y., Qi, L., Yuan, L. & Pan, W. (2020) The chemical index of alteration (CIA) as a proxy for climate change during glacial-interglacial transitions in Earth history. *Earth-Science Reviews*, *201*, 103032. https://doi.org/10.1016/j.earscirev.2019.103032

Williams, G.E. (1979) Sedimentology, stable-isotope geochemistry and palaeoenvironment of dolostones capping late Precambrian glacial sequences in Australia. *Journal of the Geological Society of Australia*, *26*, 377–386.

Williams, G.E. & Gostin, V.A. (2019) Late Cryogenian glaciation in South Australia: fluctuating ice margin and no extreme or rapid post-glacial sea-level rise. *Geoscience Frontiers*, *10*, 1397–1408.

Wynn, P.M., Fairchild, I.J., Borsato, A., Spötl, C., Hartland, A., Baker, A., Frisia, S. & Baldini, J. (2018) Sulphate partitioning into calcite: experimental verification of pH control and application to seasonality in speleothems. *Geochimica Cosmochimica Acta*, *226*, 69–83.

Xiao, S.H. & Narbonne, G.M. (2020) The Ediacaran period. In: Gradstein, F.M., Ogg, J.G., Schmitz, M. & Ogg, G. (Eds.) *Geological time scale 2020*. Amsterdam: Elsevier, pp. 521–561.

Yang, J., Jansen, M.F., Macdonald, F.A. & Abbot, D.S. (2017) Persistence of a freshwater surface ocean after a snowball. *Earth Geology*, *345*, 615–618.

Yu, W., Algeo, T.J., Zhou, Q., Du, Y. & Wang, P. (2020) Cryogenian cap carbonate models: a review and critical assessment. *Palaeogeography, Palaeoclimatology, Palaeoecology*, *552*, 109727.

Zhou, C., Bao, H., Peng, Y. & Yuan, X. (2010) Timing the deposition of ^{17}O-depleted barite at the aftermath of Nantuo glacial meltdown in South China. *Geology*, *38*, 903–906.

Zhou, C., Huyskens, M.H., Lang, S., Xiao, S. & Ying, Q.-Z. (2019) Calibrating the terminations of Cryogenian global glaciations. *Geology*, *47*, 251–254. https://doi.org/10.1130/G45719.1

SUPPORTING INFORMATION

Additional supporting information can be found online in the Supporting Information section at the end of this article.

How to cite this article: Fairchild, I. J., Bao, H., Windmill, R. & Boomer, I. (2022). The Marinoan cap carbonate of Svalbard: Syngenetic marine dolomite with ^{17}O-anomalous carbonate-associated sulphate. *The Depositional Record*, *00*, 1–26. https://doi.org/10.1002/dep2.201